Energy levels and magneto-optical transitions in parabolic quantum dots with spin-orbit coupling

Pekka Pietiläinen[1,2] and Tapash Chakraborty[1,*]

[1]*Department of Physics and Astronomy, University of Manitoba, Winnipeg, Canada R3T 2N2*
[2]*Department of Physical Sciences/Theoretical Physics, P. O. Box 3000, FIN-90014 University of Oulu, Finland*
(Received 7 September 2005; revised manuscript received 21 February 2006; published 13 April 2006)

We report on the electronic properties of few interacting electrons confined in a parabolic quantum dot based on a theoretical approach developed to investigate the influence of Bychkov-Rashba spin-orbit (SO) interaction on such a system. We note that the spin-orbit coupling profoundly influences the energy spectrum of interacting electrons in a quantum dot. Here we present accurate results for the energy levels and optical-absorption spectra for parabolic quantum dots containing up to four interacting electrons, in the presence of spin-orbit coupling and under the influence of an externally applied, perpendicular magnetic field. We have described in detail a very accurate numerical scheme to evaluate these quantities. We have evaluated the effects of the SO coupling on the Fock-Darwin spectra for quantum dots made out of three different semiconductor systems, InAs, InSb, and GaAs. The influence of SO coupling on the single-electron spectra manifests itself by primarily lifting the degeneracy at zero magnetic field, rearrangement of some of the energy levels at small magnetic fields, and level repulsions at high fields. These results are explained as due to mixing of different spinor states for increasing strength of the SO coupling. As a consequence, the corresponding absorption spectra reveal anticrossing structures in the two main lines of the spectra. For interacting many-electron systems we observed the appearance of discontinuities, anticrossings, and new modes that appear in conjunction with the two main absorption lines. These additional features arise entirely due to the SO coupling and are a consequence of level crossings and level repulsions in the energy spectra. An intricate interplay between the SO coupling and the Zeeman energies is shown to be responsible for these additional features seen in the energy spectra. Optical absorption spectra for all three types of quantum dots studied here show a common feature: new modes appear, mostly near the upper main branch of the spectra around 2 T, that become stronger with increasing SO coupling strength. Among the three types of systems considered here, the optical signature of the SO interaction is found to be the strongest in the absorption spectra of the GaAs quantum dot, but only at very large values of the SO coupling strength, and appears to be the weakest for the InSb quantum dot. Experimental observation of these modes that appear solely due to the presence of the SO coupling would provide a rare glimpse into the role of the SO coupling in nanostructured quantum systems.

I. INTRODUCTION

Impressive developments in nanofabrication technology have made it now possible to design quantum dots (QDs) and coupled quantum dots at the nanoscale. These systems comprise a few electrons that are quantum confined, for our present purpose, at the semiconductor interface to form zero-dimensional systems. What is more remarkable is that the electronic states in these systems can be precisely controlled via external voltages.[1] Magneto-optical studies of parabolic quantum dots (described as *artificial atoms*[2] by us in 1990) have been intensely explored for more than a decade[2–6] in order to understand the unique electronic and optical properties of these systems and because they are promising candidates for optoelectronic devices, applications in optical quantum information technology, etc.[7,8] As a result of these studies, a very good theoretical and experimental understanding of the single-electron states in the dot has already been achieved. At the most basic level, the solution of the Schrödinger equation for an electron confined by a harmonic potential $v_c = \frac{1}{2} m^* \omega_0 r^2$ (ω_0 is the confinement potential strength) in the presence of an external perpendicular magnetic field has been well known since the beginning of quantum mechanics.[4,9] The energy eigenvalues are evaluated from

$$E_{n\ell} = (2n + |\ell| + l)\hbar\Omega - \tfrac{1}{2}\ell\hbar\omega_c$$

where $n = 0, 1, 2, \ldots$ and $\ell = 0, \pm 1, \ldots$ are the principal and azimuthal quantum numbers, respectively, $\Omega^2 = (\omega_0^2 + \frac{1}{4}\omega_c^2)$, and ω_c is the cyclotron frequency. The energies for the dipole-allowed transitions among these levels are given by the relation[2,4,5]

$$\Delta E_{\pm} = \hbar\Omega \pm \tfrac{1}{2}\hbar\omega_c.$$

A variety of experiments[3,4,6] have subsequently established this energy relation to a great accuracy. One surprising observation here was that the magnetic-field-dependent far-intrared (FIR) absorption in quantum dots containing more than one electron was found to be essentially *independent* of the number of electrons confined and instead was largely determined by the above relation for $\Delta E_{\pm}$.[5] Quite obviously, this means that magneto-optical spectroscopy does not provide any relevant information about the role of mutual interactions among the confined electrons. That puzzling observation of Ref. 5 was later resolved by Maksym and Chakraborty,[2–4,10] who pointed out that for a parabolic QD in an external magnetic field, the dipole interaction is a function of the center-of-mass (c.m.) coordinate alone and the inter-electron interaction remains totally ineffective. This some-

what disappointing performance of a parabolic dot notwithstanding, FIR spectroscopy of QDs (parabolic or otherwise) has generated enormous interest for over a decade that is yet to subside.[6] We have now included another interesting element into the problem, the spin-orbit (SO) interaction. In this paper, we have presented detailed evidence to support the fact that in the presence of spin-orbit coupling, magneto-optical transitions show many additional interesting features that can in fact, be tuned by the SO coupling. Based on these results, we propose that magneto-optical transitions are best suited to determine optically the unique effect of the SO coupling in quantum dots described below.[11]

The SO coupling in nanostructured systems such as semiconductor QDs is of late receiving increasing attention because of its relevance to spin transport in low-dimensional electron channels.[12,13] A major goal of this type of work is to find ways to tune the SO field and thereby coherently manipulate electron spins in quantum dots.[14–31] One possible outcome of this type of research would be a better understanding of spin dynamics in the QDs that will facilitate future electronic and information processing, especially in quantum computing and quantum communication.[32] Spin degree of freedom is perhaps more advantageous than charge because unlike charge, spin is not coupled to electromagnetic noise and therefore has a much longer coherence time.[33] Coherent manipulation of electron spin via optical excitations has indeed been demonstrated in self-assembled InAs/GaAs quantum dots, and the single-electron spin-flip time has been measured to be ~15 ns albeit at a low temperature (10 K).[34] Given the obvious importance of the electron spin states in nanostructures, an improved knowledge of the influence of spin-orbit coupling on electronic states in quantum dots is quite essential in this pursuit. Most of the experimental effort to date reported in the literature have focused on magnetotransport measurements.[35] In this work (and in Ref. 11), we report our detailed study of optical-absorption spectra that are experimentally observable and could, in principle, provide an important probe of SO interaction in few-electron quantum dots.

The spin-orbit interaction in semiconductor heterostructures can be caused by an electric field perpendicular to the two-dimensional electron gas (2DEG). Riding on an electron, this electric field will be experienced as an effective magnetic field lying in the plane of the 2DEG, perpendicular to the wave vector k of the electron. The effective Zeeman interaction of the electron spin with the field lifts the spin degeneracy (internal Zeeman effect). This is usually referred to in the literature as the Bychkov-Rashba mechanism. This results in an isotropic spin splitting energy Δ_{SO} at $B=0$ proportional to k.[36]

Let us consider an electron in the 2DEG moving with a velocity $\vec{v}$ in the presence of an electric field $\vec{E}$. In the rest frame of the electron, this transforms (relativistically) into an effective magnetic field $\vec{B}_{eff}$,

$$\vec{B}_{eff} = -\frac{1}{2c^2}\vec{v}\times\vec{E},$$

where c is the speed of light. The magnetic moment of the electron will then couple to $\vec{B}_{eff}$. The resulting spin-orbit interaction is

$$\mathcal{H}_{SO} = \vec{\mu}\cdot\vec{B}_{eff} = -\frac{1}{2c^2}\vec{\mu}\cdot(\vec{v}\times\vec{E}) = \frac{e\hbar^2}{4m_0^2c^2}\vec{\sigma}\cdot(\vec{k}\times\vec{E})$$

since $\vec{\mu}=-(e\hbar/2m_0)\vec{\sigma}$ and $\vec{v}=\hbar\vec{k}/m_0$. It can be rewritten as

$$\mathcal{H}_{SO} = \frac{e\hbar^2}{4m_0^2c^2}\vec{\sigma}\cdot(\vec{k}\times\vec{E}) = \alpha'\langle E_z\rangle(-i\vec{\nabla}\times\vec{\sigma})_z, \quad (1)$$

where the electric field is aligned along the z axis.

Alternatively, a general spin-orbit Hamiltonian that stems directly from the quadratic in v/c expansion of the Dirac equation is[37]

$$\mathcal{H}_{SO} = \frac{e\hbar}{(2m_0c)^2}\vec{\nabla}V(\vec{r})\cdot(\vec{\sigma}\times\vec{p}). \quad (2)$$

The electric field associated with $V(\vec{r})$ is $\vec{E}(\vec{r})=\vec{\nabla}V(\vec{r})$, and is directed along the z direction. The spin-orbit interaction Hamiltonian

$$\mathcal{H}_{SO} = \frac{e\hbar^2}{(2m_0c)^2}\langle E_z\rangle\frac{1}{\hbar}(\vec{\sigma}\times\vec{p})\cdot\hat{n}$$

$$= \alpha'\langle E_z\rangle\frac{1}{\hbar}(\vec{\sigma}\times\vec{p})\cdot\hat{n}$$

$$= \alpha'\langle E_z\rangle(\vec{\sigma}\times\vec{k})\cdot\hat{n},$$

where $\alpha'=e(\hbar/2m_0c)^2$ is then identical to the factor in Eq. (1). An important point to note here is that a nonvanishing gradient in Eq. (2) requires that the system must have inversion asymmetry. In the present case that arises from the structural inversion asymmetry.[38] The form of the spin-orbit interaction that we have dealt with in this paper is therefore described by the Hamiltonian

$$\mathcal{H}_{SO} = \alpha(\vec{k}\times\vec{\sigma})_z = i\alpha\left(\sigma_y\frac{\partial}{\partial x} - \sigma_x\frac{\partial}{\partial y}\right), \quad (3)$$

where the z axis is chosen perpendicular to the 2DEG (in the xy plane), α is the spin-orbit coupling constant, which is sample dependent and is proportional to the interface electric field that confines the electrons in the x-y plane, $\vec{\sigma}=(\sigma_x,\sigma_y,\sigma_z)$ denotes the Pauli matrices, and $\vec{k}$ is the planar wave vector. This is the Bychkov-Rashba Hamiltonian[36] that has been receiving of late rather widespread attention.[35]

The single-electron Hamiltonian for the 2DEG including the Bychkov-Rashba term has the form

$$\mathcal{H} = \frac{\vec{p}^2}{2m^*} + \frac{\alpha}{\hbar}(\vec{\sigma}\times\vec{p})_z$$

$$= -\frac{\hbar^2}{2m^*}\vec{\nabla}^2 + i\alpha\left(\sigma_y\frac{\partial}{\partial x} - \sigma_x\frac{\partial}{\partial y}\right)$$

$$= \begin{pmatrix} -\dfrac{\hbar^2}{2m^*}\vec{\nabla}^2 & \alpha\nabla^- \\[2ex] -\alpha\nabla^+ & -\dfrac{\hbar^2}{2m^*}\vec{\nabla}^2 \end{pmatrix}$$

where $\vec{\nabla}^2=\partial^2/\partial x^2+\partial^2/\partial y^2$ and $\nabla^{\pm}=\partial/\partial x\pm i\partial/\partial y$.

Since the operators $\hat{p}_x$ and $\hat{p}_y$ commute with the Hamiltonian, we can search for $\alpha \neq 0$ eigenstates of the form

$$\Psi(k_x,k_y) = e^{ik_x x + ik_y y}\sum_\sigma C^\sigma |\sigma\rangle = e^{ik_x x + ik_y y}\begin{pmatrix} C^+ \\ C^- \end{pmatrix},$$

with $|\sigma\rangle = \begin{pmatrix} 1 \\ 0 \end{pmatrix}$ (spin up) or $\begin{pmatrix} 0 \\ 1 \end{pmatrix}$ (spin down). Solutions of

$$\mathcal{H}\Psi(k_x,k_y) = \mathcal{E}\Psi(k_x,k_y)$$

are readily obtained as[39]

$$\Psi^\pm(k_x,k_y) = \frac{1}{\sqrt{2}}\begin{pmatrix} 1 \\ \dfrac{\pm k_y \mp ik_x}{k} \end{pmatrix}e^{ik_x x + ik_y y}.$$

The energy dispersion then consists of two branches

$$\mathcal{E}^\pm(k) = \frac{\hbar^2}{2m^*}k^2 \pm \alpha k$$

with an energy separation $\Delta_{SO} = \mathcal{E}^+ - \mathcal{E}^- = 2\alpha k$ for a given k. The spin parts of the wave functions $\chi^\pm(k_x,k_y)$ are mutually orthogonal and $\langle \chi^\pm | \sigma_z | \chi^\pm \rangle = 0$. Therefore in the states $\Psi^\pm$ the spins of the electrons lie in the xy plane and point in opposite directions. In addition,

$$\langle \chi^\pm | \sigma_x | \chi^\pm \rangle = \frac{2k_y}{k}, \quad \langle \chi^\pm | \sigma_y | \chi^\pm \rangle = -\frac{2k_x}{k},$$

i.e., the spins are *perpendicular* to the momentum (k_x,k_y). The spatial alignment of spins therefore depends on the wave vector.[12,36] The Fermi surface is a pair of concentric circles with radii $k_{F,\max}$ and $k_{F,\min}$. In the present paper, we are dealing with systems having rotational symmetry. The formalism in that case is derived in detail in Sec. II.

Experimentally observed values of the SO coupling strength α, based on the investigation of the Shubnikov–de Haas oscillations in a 2DEG confined at the heterojunctions with a narrow-gap quantum well (e.g., InGaAs/InAlAs, InAs/GaSb, etc.), have been established to lie in the range of 5–45 meV nm.[35] In this range of α the energy levels and magnetization in the ground state of two interacting electrons confined in a parabolic quantum dot in an external magnetic field were recently reported by us.[31]

Our paper is organized as follows. In Sec. II, we present the essential formalism for our study of noninteracting electrons in parabolic QDs in the presence of the spin-orbit interaction. The single-electron basis and the dipole matrix elements are derived here. We also explain why the dipole-allowed transitions are so significantly influenced by the presence or absence of the SO interaction. The classic Fock-Darwin spectra for three different quantum dot systems (InAs, InSb, and GaAs) with or without the SO coupling are presented and discussed in detail. The formalism for the many-electron system in a spin-orbit-coupled parabolic QD is presented in Sec. III. The complexities of introducing the SO coupling, in particular for interacting electrons, are made clear in Sec. III. The task of finding a suitable numerical technique is even more challenging, and an approach that is appropriate for our purpose is described in the Appendix. Numerical results for the energy levels and the optical-

absorption spectra for the three types of QDs containing up to four interacting electrons are presented and discussed in Sec. IV. It should be pointed out that the low-lying energy levels calculated here for single- and multielectron quantum dots can, in principle, be observed in transport,[40] or capacitance spectroscopy.[41] Given the accute interest in the influence of the SO coupling in nanostructured systems and the resulting intense activities on this topic, it is no surprise that many different theoretical techniques have been put forward in the literature. To view our work in proper perspective, we present a brief review of many of those theoretical papers in Sec. V. We conclude with a brief outlook for future work along this direction in Sec. VI. For a brief account of our earlier work on the SO coupling effects in parabolic QDs, see Refs. 11 and 31.

II. SINGLE-ELECTRON PICTURE

The Hamiltonian for an electron in a parabolic confinement and under external magnetic field is given by

$$\mathcal{H}_0 = \frac{1}{2m^*}\left(\vec{p} - \frac{e}{c}\vec{A}\right)^2 + \frac{1}{2}m^*\omega_0^2 r^2 + \frac{\alpha}{\hbar}\left[\vec{\sigma}\times\left(\vec{p} - \frac{e}{c}\vec{A}\right)\right]_z$$

$$+ \frac{1}{2}g\mu_B B\sigma_z. \tag{4}$$

Here $\vec{\sigma}$ is the vector of Pauli matrices, i.e.,

$$\vec{\sigma} = \sigma_x\vec{i} + \sigma_y\vec{j} + \sigma_z\vec{k} = \begin{pmatrix} 0 & 1 \\ 1 & 0 \end{pmatrix}\vec{i} + \begin{pmatrix} 0 & -i \\ i & 0 \end{pmatrix}\vec{j} + \begin{pmatrix} 1 & 0 \\ 0 & -1 \end{pmatrix}\vec{k}. \tag{5}$$

We work in the symmetric gauge and the vector potential corresponding to the external perpendicular magnetic field is

$$\vec{A} = \frac{B}{2}(-y,x,0). \tag{6}$$

The term $(\alpha/\hbar)[\vec{\sigma}\times(\vec{p} - e\vec{A}/c)]_z$ in the Hamiltonian is the spin-orbit coupling due to the inhomogenous potential confining the electrons to the 2D plane and possible external gate voltages applied on the top of the dot. The parameter α determines the strength of this coupling and in the case of external gate voltages its magnitude can be varied. Finally, the last term $\frac{1}{2}g\mu_B B\sigma_z$ is the ordinary Zeeman coupling, g being the effective Landé g factor.

The eigenstates of the single-particle problem

$$\mathcal{H}_0\phi = \varepsilon\phi \tag{7}$$

are clearly two-component spinors

$$|\lambda\rangle = \begin{pmatrix} \phi^\uparrow \\ \phi^\downarrow \end{pmatrix}. \tag{8}$$

Writing Eq. (7) in polar coordinates and substituting a trial wave function of the form

$$\phi = \begin{pmatrix} f^{\uparrow}(r)e^{i\ell^{\uparrow}\theta} \\ f^{\downarrow}(r)e^{i\ell^{\downarrow}\theta} \end{pmatrix} \qquad (9)$$

it is easy to see that the quantum numbers $\ell^{\uparrow}$ and $\ell^{\downarrow}$ must be integers and that they depend on each other in the way

$$\ell^{\uparrow} = \ell^{\downarrow} - 1. \qquad (10)$$

Hence we need only one quantum number for the angular motion, i.e., solutions of the single-particle equation (7) are of the form

$$|\lambda\rangle = |k,\ell\rangle = \begin{pmatrix} f_{k,\ell}^{\uparrow}(r)e^{i\ell\theta} \\ f_{k,\ell}^{\downarrow}(r)e^{i(\ell+1)\theta} \end{pmatrix}. \qquad (11)$$

Here the quantum number k is associated with the radial motion (and not to be confused with the wave vector described in Sec. I). The form of the spinor (11) simply restates the fact that under the SO coupling the good quantum numbers are related to $\vec{L}+\vec{S}$. In our case the conserved quantity is

$$j = \ell^{\uparrow,\downarrow} + s_z^{\uparrow,\downarrow} = \ell + \tfrac{1}{2} \qquad (12)$$

where $s_z = \pm\tfrac{1}{2}$ depending on the component of the spinor, i.e., $+\tfrac{1}{2}$ for the upper component and $-\tfrac{1}{2}$ for the lower one.

In order to find the radial wave functions $f^{\uparrow,\downarrow}$ we transform to dimensionless units by setting

$$\omega_c = \frac{eB}{m^*c}, \quad a^2 = \frac{\hbar}{m^*\omega_0(1+\omega_c^2/4\omega_0^2)^{1/2}},$$

$$x = \frac{r^2}{a^2}, \quad \beta = \frac{m^*\alpha a}{\hbar^2},$$

$$b_R = \frac{ea^2B}{\hbar^2}, \quad \eta^{\pm} = 1 \pm 2b_R,$$

$$\nu_{\ell}^{\uparrow,\downarrow} = \frac{\ell\omega_c}{4\omega_0(1+\omega_c^2/4\omega_0^2)^{1/2}} \pm \frac{g\mu_B B}{4\hbar\omega_0(1+\omega_c^2/4\omega_0^2)^{1/2}},$$

$$\varepsilon = 2\hbar\omega_0\left(1+\frac{\omega_c^2}{4\omega_0^2}\right)^{1/2}\nu, \quad g^{\uparrow,\downarrow}(x) = f^{\uparrow,\downarrow}(r).$$

Substituting these into the Hamiltonian (4) the radial part of Eq. (7) takes the form

$$xg^{\uparrow\prime\prime} + g^{\uparrow\prime} + \left(\nu - \frac{\ell^2}{4x} - \frac{x}{4} + \nu_{\ell}^{\uparrow}\right)g^{\uparrow}$$
$$- \beta x^{1/2}\left(g^{\downarrow\prime} + \frac{\ell+1}{2x}g^{\downarrow} + b_R g^{\downarrow}\right) = 0, \qquad (13)$$

$$xg^{\downarrow\prime\prime} + g^{\downarrow\prime} + \left(\nu - \frac{(\ell+1)^2}{4x} - \frac{x}{4} + \nu_{\ell+1}^{\downarrow}\right)g^{\downarrow}$$
$$+ \beta x^{1/2}\left(g^{\uparrow\prime} - \frac{\ell}{2x}g^{\uparrow} - b_R g^{\uparrow}\right) = 0 \qquad (14)$$

of two coupled differential equations. For $\beta=0$ (i.e., $\alpha=0$) these equations describe radial motions of two independent

two-dimensional harmonic oscillators with eigenvalues

$$\nu_{n\ell}^{\uparrow,\downarrow} = n + \frac{|\ell|+1}{2} + \nu_{\ell}^{\uparrow,\downarrow} \qquad (15)$$

and eigenfunctions

$$g_{n\ell} = \sqrt{\frac{n!}{(n+|\ell|)!}}e^{-x/2}x^{|\ell|/2}L_n^{|\ell|}(x). \qquad (16)$$

Here $L_n^{|\ell|}$ is the associated Laguerre polynomial. Therefore it is logical to seek the solution for Eqs. (13) and (14) in the form of the expansion[14]

$$g^{\uparrow,\downarrow} = \sum_{n=0} c_{n,\ell}^{\uparrow,\downarrow}g_{n,\ell}. \qquad (17)$$

In spinor language (9) this corresponds to the expansion

$$|\lambda\rangle = \begin{pmatrix} \displaystyle\sum_{n=0} c_{n,\ell}^{\uparrow}g_{n,\ell}(x)e^{i\ell\theta} \\ \displaystyle\sum_{n=0} c_{n,\ell+1}^{\downarrow}g_{n,\ell+1}(x)e^{i(\ell+1)\theta} \end{pmatrix}$$
$$= e^{i\ell\theta}\sum_{n=0} c_{n,\ell}^{\uparrow}\begin{pmatrix} g_{n,\ell}(x) \\ 0 \end{pmatrix} + e^{i(\ell+1)\theta}\sum_{n=0} c_{n,\ell+1}^{\downarrow}\begin{pmatrix} 0 \\ g_{n,\ell+1}(x) \end{pmatrix}. \qquad (18)$$

The coefficents $c_{n,\ell}^{\uparrow,\downarrow}$ can be obtained by minimizing the expectation value $\langle\lambda|\mathcal{H}_0|\lambda\rangle$. At this point it is usefull to relabel our spinors. For example, for non-negative values of ℓ we set

$$u_{2n} = e^{i\ell\theta}\begin{pmatrix} g_{n,\ell}(x) \\ 0 \end{pmatrix}, \qquad (19)$$

$$u_{2n+1} = e^{i(\ell+1)\theta}\begin{pmatrix} 0 \\ g_{n,\ell+1}(x) \end{pmatrix}, \qquad (20)$$

$$z_{2n} = c_{n,\ell}^{\uparrow}, \qquad (21)$$

$$z_{2n+1} = c_{n,\ell+1}^{\downarrow}. \qquad (22)$$

The minimization of

$$\langle\lambda|\mathcal{H}_0|\lambda\rangle = \sum_{n,n'} z_{n'}z_n\langle u_{n'}|\mathcal{H}_0|u_n\rangle$$

leads now to the diagonalization of the symmetric tridiagonal matrix $\mathcal{H}$ with diagonal

$$\mathrm{diag}\,\mathcal{H} = (\nu_{0,\ell}^{\uparrow}, \nu_{0,\ell+1}^{\downarrow}, \ldots, \nu_{n,\ell}^{\uparrow}, \nu_{n,\ell+1}^{\downarrow}, \ldots) \qquad (23)$$

and subdiagonal

$$\mathrm{subdiag}\,\mathcal{H} = \frac{\beta}{2}(0, \sqrt{\ell+1}\,\eta^+, \eta^-, \ldots, \sqrt{n}\,\eta^-,$$
$$\sqrt{n+\ell+1}\,\eta^+, \sqrt{n+1}\,\eta^-, \ldots). \qquad (24)$$

The diagonalization yields a set of solutions: the set $\{\nu^{(k,\ell)}\}$ of eigenvalues and the set $\{z_n^{(k,\ell)}\}$ of eigenvectors indexed by the particular solution k and the fixed angular momentum ℓ. These are the energies of the spinors and the

expansion coefficients (21) and (22). For negative values of ℓ the tridiagonal matrix consists of the diagonal

$$\text{diag } \mathcal{H} = (\nu_{0,\ell+1}^\downarrow, \nu_{0,\ell}^\uparrow, \dots, \nu_{n,\ell+1}^\downarrow, \nu_{n,\ell}^\uparrow, \dots) \qquad (25)$$

and the subdiagonal

$$\text{subdiag } \mathcal{H} = -\frac{\beta}{2}(0, \sqrt{|\ell|}\,\eta^-, \eta^+, \dots, \sqrt{n}\,\eta^+,$$
$$\sqrt{n+|\ell|}\,\eta^-, \sqrt{n+1}\,\eta^+, \dots). \qquad (26)$$

The spinors thus obtained comprise our single-particle basis

$$\mathcal{B}_S = \{|\lambda_i\rangle | i = 0, 1, 2, \dots\}$$
$$= \{|k,\ell\rangle | k = 0, 1, 2, \dots; \ell = 0, \pm 1, \pm 2, \dots\}. \qquad (27)$$

A. Dipole matrix elements

According to the Fermi golden rule the intensity of absorption in dipole approximation is proportional to the square of the matrix element

$$I = \langle f | \sum_{i=1}^{N} r_i e^{\pm i\theta_i} | i \rangle$$

when the transition goes from the initial N-particle state $|i\rangle$ to the final state $|f\rangle$. To evaluate this we need to know the dipole matrix elements $d_{\lambda',\lambda}$ between the spinor states $|\lambda'\rangle$ and $|\lambda\rangle$, i.e., the elements

$$d_{\lambda',\lambda} = \langle \lambda' | re^{\pm i\theta} | \lambda \rangle = \langle k', \ell' | re^{\pm i\theta} | k, \ell \rangle. \qquad (28)$$

For simplicity we consider only the circular polarization $e^{+i\theta}$ (the other circular polarization is obtained by reversing the roles of λ and λ'). Substituting expansions (17) into the above expression (28) we get

$$d_{\lambda',\lambda} = a\delta_{\ell',\ell+1}\sum_n (c_n'^\uparrow c_n^\uparrow \sqrt{n+\ell+1} - c_{n-1}'^\uparrow c_n^\uparrow \sqrt{n}$$
$$+ c_n'^\downarrow c_n^\downarrow \sqrt{n+\ell+2} - c_{n-1}'^\downarrow c_n^\downarrow \sqrt{n}) \qquad (29)$$

when $\ell \geq 0$,

$$d_{\lambda',\lambda} = a\delta_{\ell',0}\sum_n (c_n'^\uparrow c_n^\uparrow \sqrt{n+1} - c_{n+1}'^\uparrow c_n^\uparrow \sqrt{n+1} + c_n'^\downarrow c_n^\downarrow \sqrt{n+1}$$
$$- c_{n-1}'^\downarrow c_n^\downarrow \sqrt{n}) \qquad (30)$$

when $\ell = -1$, and

$$d_{\lambda',\lambda} = a\delta_{\ell',\ell+1}\sum_n (c_n'^\uparrow c_n^\uparrow \sqrt{n-\ell} - c_{n+1}'^\uparrow c_n^\uparrow \sqrt{n+1}$$
$$+ c_n'^\downarrow c_n^\downarrow \sqrt{n-\ell-1} - c_{n+1}'^\downarrow c_n^\downarrow \sqrt{n+1}) \qquad (31)$$

when $\ell < -1$. The intensity is then obtained from $I \propto |d_{\lambda_1\lambda_2}|^2$.[42] In all our figures for the absorption spectra, the size of the points is proportional to the calculated intensity.

Dipole-allowed transitions in a parabolically confined quantum dot can be very different in the presence of the SO interaction. This important fact can readily be understood from the following arguments. When subjected to the radia-

tion field with amplitude a and polarization $\vec{\epsilon}$, the vector potential $\vec{A}$ in the single-particle Hamiltonian

$$\mathcal{H}_0 = \frac{1}{2m^*}\left(\vec{p} - \frac{e}{c}\vec{A}\right)^2 + \frac{1}{2}m^*\omega_0^2 r^2 + \frac{\alpha}{\hbar}\left[\vec{\sigma} \times \left(\vec{p} - \frac{e}{c}\vec{A}\right)\right]_z$$
$$+ \frac{1}{2}g\mu_B B\sigma_z$$

should be replaced by the potential

$$\vec{A} \rightarrow \vec{A} + \vec{A}_\omega, \vec{A}_\omega = \vec{\epsilon}ae^{i\vec{k}\cdot\vec{r}-i\omega t}.$$

In the dipole approximation we assume that

$$A_\omega \approx \vec{\epsilon}ae^{-i\omega t}$$

and correspondingly the Hamiltonian will be[43]

$$\mathcal{H} \approx \mathcal{H}_0 - \mathcal{H}'e^{-i\omega t},$$

where

$$\mathcal{H}' = \frac{ea}{m^*c}\vec{\epsilon}\cdot\left(\vec{p} - \frac{e}{c}\vec{A}\right) + \frac{\alpha ea}{\hbar c}[\vec{\sigma} \times \vec{\epsilon}]_z.$$

In a many-body system when $\alpha = 0$ the first term generates the c.m. density excitations where mutual interactions play no role. Consequently (in dipole approximation) only transitions between these modes are possible. When α is different from zero, the second term ($\propto \sigma_x\epsilon_y - \sigma_y\epsilon_x$) in $\mathcal{H}'$ can create spin-density oscillations and interactions have observable effects on their properties. We should point out here that in SO-coupled systems the dipole operator retains its familiar form $\hat{Q} = (ea/c)\vec{\epsilon}\cdot\vec{r}$. This can be easily verified by evaluating its commutator with the Hamiltonian $\mathcal{H}_0$

$$[\hat{Q}, \mathcal{H}_0] = i\hbar\mathcal{H}'.$$

The dipole operator is in fact independent of the electron spin. The dipole-allowed optical transitions are always between the same spin states, only the angular momenta must differ by unity. In the presence of the SO coupling, neither the dipole operator nor the selection rule changes, but the SO interaction mixes the neighboring angular momentum values (ℓ and $\ell+1$) as well as the spin and hence the selection rule now applies to the total angular momentum J as well. Therefore, in the presence of the SO coupling, transitions from other states that are not allowed when $\alpha = 0$ should now be observable.

B. Fock-Darwin spectra

In our numerical investigations, we choose InAs, InSb, and GaAs quantum dots with parameters $m^*/m_0 = 0.042$, $\epsilon = 14.6$, $g = -14$, $m^*/m_0 = 0.014$, $\epsilon = 17.88$, $g = -40$, and $m^*/m_0 = 0.063$, $\epsilon = 12.9$, $g = -0.44$, respectively. We would like to stress here that we are investigating the properties of planar quantum dots that are carved out of two-dimensional heterostructures. Electrons occupying the dots are assumed to originate from a single band of the host material. Provided that the excitation energies that we are concerned with are significantly smaller than the band gap of the material, the
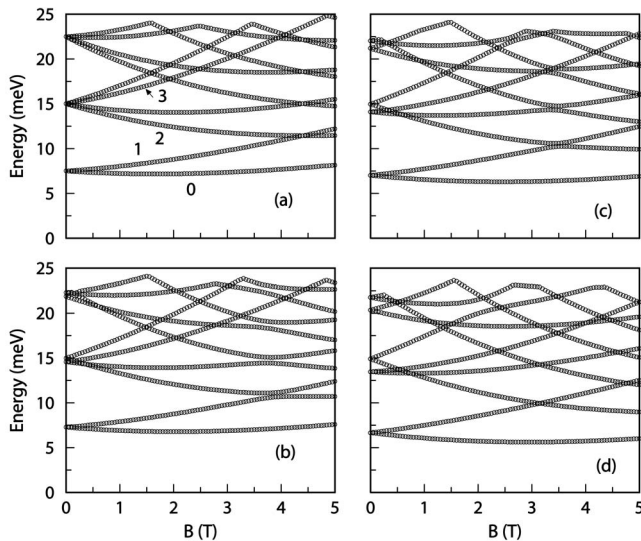
FIG. 1. Some of the low-lying energy states for noninteracting electrons confined in an InAs quantum dot for various values of the SO coupling strength (in meV nm) $\alpha=0$ (a) 20 (b) 30 (c), and 40 (d). The labels in (a) are explained in the text.

single-band approximation is supposed to work quite well. Consequently, the band structure properties are, to a good approximation, incorporated into a single effective-mass parameter. Nonparabolicity of the conduction band in narrow-gap semiconductors[44] such as InAs and InSb may have some minor effects on the numerical results presented. Similar types of arguments apply for the other material parameters as well. Another approximation that is used here, and is also routinely used in the literature, involves the assumption that the electrons are confined strictly into a two-dimensional plane. The materials and the range of excitation energies of the system that is of interest to us are such that the electrons can be considered to remain in the lowest subband (due to the confinement). Nevertheless, it is still true that the electron wave functions have a finite *spread* in the direction perpendicular to the 2D heterostructure plane. As long as all the electrons stay on the lowest subband, they all exhibit exactly the same behavior in the perpendicular direction. Therefore, the effect of spreading of the wave function on the single-particle properties is practically negligible. The spreading would primarily influence the many-electron states by making the Coulomb interaction somewhat softer. However, the amount of softening would be practically independent of the states of the interacting electrons. As a result we would merely see an overall shift in the energies.

Although the InAs quantum structures have been the system of choice for investigation of spin-related phenomena,[35] InSb quantum dots are interesting for their very high g values and a relatively large α ($\sim$14 meV nm).[45] For the GaAs quantum dots, the observed value of α is $\sim$6 meV nm.[28] In all these systems we consider the confinement potential strength to be $\hbar\omega_0=7.5$ meV. Some of the low-lying states of the Fock-Darwin spectra of the InAs, InSb, and GaAs QDs are shown in Figs. 1–3, respectively and the corresponding optical-absorption spectra in these systems are presented in Figs. 4–6.
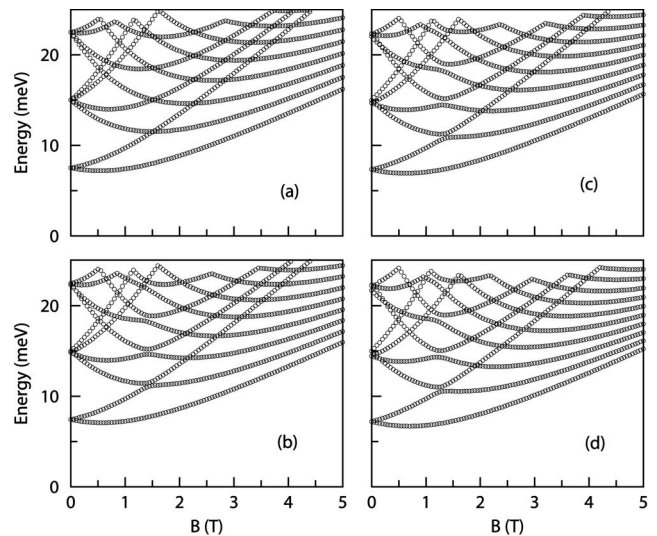

FIG. 2. Some of the low-lying energy states for noninteracting electrons confined in a InSb quantum dot for various values of the SO coupling strength (in meV.nm), $\alpha=0$ [a], $\alpha=20$ [b], $\alpha=30$ [c], and $\alpha=40$ [d].

As compared to the Fock-Darwin spectra of quantum dots without the SO coupling [shown in Figs. 1(a), 2(a), and 3(a)] the most outstanding features in the energy spectra of quantum dots with the SO coupling are the *lifting of degeneracy* at vanishing magnetic field, rearrangement of some of the levels at small fields, and level repulsions at higher magnetic fields. To gain some insight into the mechanism causing this type of behavior, let us have a closer look, as an example, at the energy levels involved in the lowest absorption lines of the InAs dot [curves labeled 0–3 in Fig. 1(a)].

In the absence of SO coupling, energies of these levels are given by the formula (15). The corresponding spinors (schematic) are displayed in Table I, where the numbers in the first
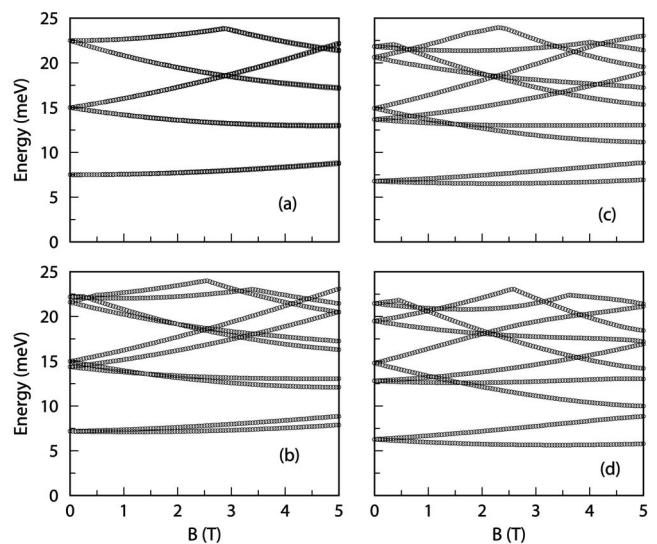

FIG. 3. Some of the low-lying energy states for noninteracting electrons confined in a GaAs quantum dot for various values of the SO coupling strength (in meV nm) $\alpha=0$ (a), 20 (b), 30 (c), and 40 (d).
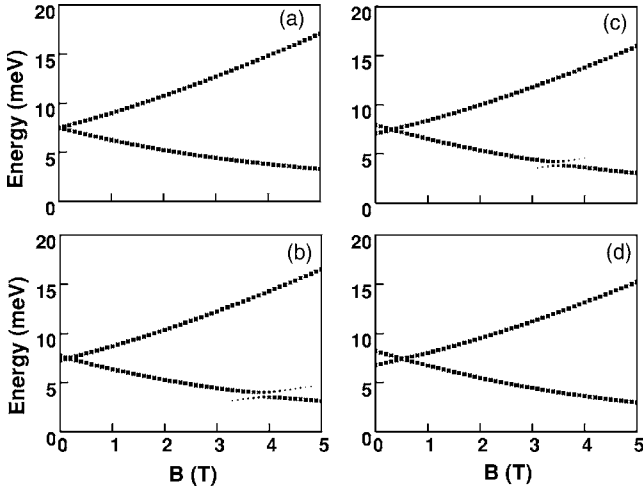
FIG. 4. Optical-absorption spectra for noninteracting electrons confined in an InAs quantum dot for various values of the SO coupling strength (in meV nm) $\alpha=0$ (a), 20 (b), 30 (c), and 40 (d).

FIG. 6. Optical-absorption spectra for noninteracting electrons confined in a GaAs quantum dot for various values of the SO coupling strength (in meV nm) $\alpha=0$ (a), 20 (b), 30 (c), and 40 (d).

column refer to the labels in Fig. 1(a). The spinors for electrons with negative and positive Landé g factors are shown in the middle and third columns, respectively. In actual physical systems, conventionally only the spinors with $g<0$ are of any interest.

The spinor states of electrons on lines 0 and 1 of Fig. 1(a) differ only by the orientation of the spin: on line 0 the spin is parallel to the magnetic field ($\parallel\hat{z}$) while on line 1 the spin is antiparallel to the field. Thus the energy difference between these states is the Zeemen splitting. The total single-particle angular momenta (12) are correspondingly $j=\pm\frac{1}{2}$. Since under the SO coupling j is a good quantum number these two states will never mix even when the SO coupling is on. When the coupling strength α increases, the higher-lying states with $j=\frac{1}{2}$ couple to the state 0 and also states with $j=-\frac{1}{2}$ couple with the state 1. In Fig. 1 this shows up as an increasing splitting of the lines 0 and 1 when going through the panels from (a) to (d). It should be noted, however, that
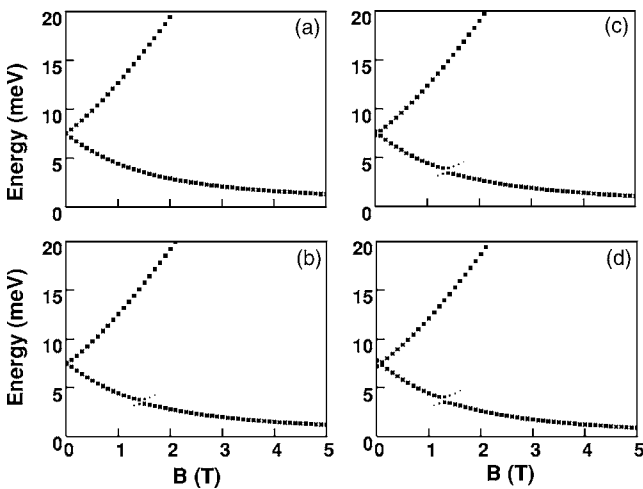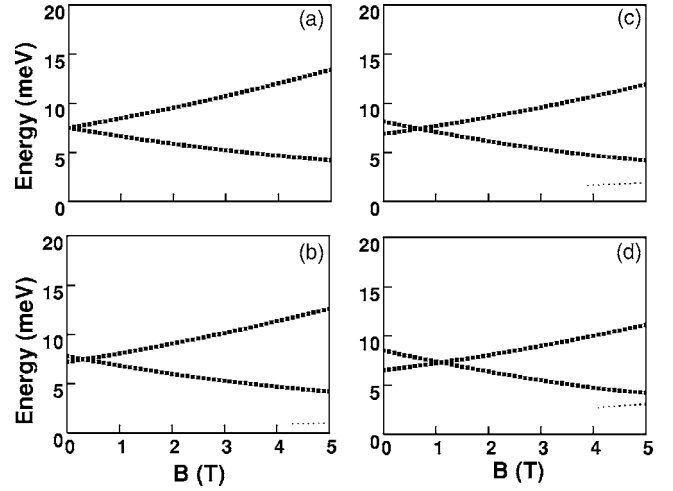
the mixing has a very minor effect on the ground state since the other states with $j=\frac{1}{2}$ are energetically very far from that.

Turning now our attention to electrons on lines 1 and 2 we see from Table I (column $g<0$) that their spinor states both have the same angular momentum $j=\ell+\frac{1}{2}=-\frac{1}{2}$. Consequently the SO interaction can mix these states. The mixing is particularly pronounced when the states are nearly degenerate, i.e., in the vicinity of the crossing point of lines 1 and 2. At moderate coupling strengths this mixing leads to level repulsions as shown in Figs. 1(b) and 1(c). When the coupling is very strong, energetically higher states with $j=-\frac{1}{2}$ also become important in the mixing, leading to the imperceptibility of the level repulsion in Fig. 1(d).

TABLE I. Schematic spinors corresponding to four Fock-Darwing levels, marked 0–3 in Fig. 1(a), of an InAs dot without SO coupling. The black squares stand for nonzero radial wave functions.

	$g<0$	$g>0$
0	$\begin{pmatrix} \blacksquare e^{i0} \\ 0e^{i\theta} \end{pmatrix}$	$\begin{pmatrix} 0e^{-i\theta} \\ \blacksquare e^{i0} \end{pmatrix}$
1	$\begin{pmatrix} 0e^{-i\theta} \\ \blacksquare e^{i0} \end{pmatrix}$	$\begin{pmatrix} \blacksquare e^{i0} \\ 0e^{i\theta} \end{pmatrix}$
2	$\begin{pmatrix} \blacksquare e^{-i\theta} \\ 0e^{i0} \end{pmatrix}$	$\begin{pmatrix} 0e^{-2i\theta} \\ \blacksquare e^{-i\theta} \end{pmatrix}$
3	$\begin{pmatrix} \blacksquare e^{i\theta} \\ 0e^{2i\theta} \end{pmatrix}$	$\begin{pmatrix} 0e^{i0} \\ \blacksquare e^{i\theta} \end{pmatrix}$

FIG. 5. Optical-absorption spectra for noninteracting electrons confined in an InSb quantum dot for various values of the SO coupling strength (in meV nm) $\alpha=0$ (a), 20 (b), 30 (c), and 40 (d).

We also mentioned lifting of degeneracies and rearrangements of energy levels as features of the SO coupling under small magnetic fields. Since we are interested in absorption, the most important states for us are the ones that can be reached from the ground state $\left(j=\frac{1}{2}\right)$ respecting the dipole transition selection rule $\Delta j = \pm 1$. These are the lowest states with $j = -\frac{1}{2}$ and $j = \frac{3}{2}$ corresponding to the lines 2 and 3 in Fig. 1(a) and to the spinors 2 and 3 (with $g < 0$) in Table I, respectively, for vanishing SO coupling. Since, as the SO interaction becomes stronger the larger is the (angular) momentum of the electron, the spinor 3 possessing maximum orbital angular momentum 2 is affected more than the spinor 2. Hence, although the energies of both spinors are decreased by the SO coupling the effect on the spinor 3 is larger.

Keeping the above discussions in mind it is now easy to interpret the features introduced by the SO coupling into the absorption spectra (Figs. 4–6). First, although the lower absorption branch consists mainly of transitions from the state 0 to the state 2 it shows an anticrossing at moderate coupling strengths. This is a direct consequence of the mixing of the spinor states 1 and 2, which results in two spinors, both with nonzero upper component. Thus we can see transitions from the ground state 0 to both of these. Furthermore, as mentioned earlier the level repulsion between states 1 and 2 resumes the form of a level crossing when the SO interaction becomes very strong. This causes the anticrossing in the absorption spectra to disappear. In the InAs dot this happens already at $\alpha = 40$ while in the InSb dot the anticrossing still persists. Since the Landé g factor of GaAs is very small the Zeeman-split state 1 does not meet the state 2 within the range of the magnetic field under consideration. Consequently we see at the lower right corners of Figs. 6(b)–6(d) only the beginnings of the lower branches of these anticrossings.

Second, the upper absorption branch corresponds mainly to transitions from the state 0 to the state 3 modified by the SO coupling. The small magnetic field, however, makes an exception. As we discussed above, at small fields the state 3 is energetically lower than the state 2 due to the SO interaction. Thus we get a crossing of spectra at small fields.

From Eq. (15), the separation between the states 2 and 3, and hence also the gap between the absorption line branches, is roughly proportional to the cyclotron frequency ω_c which in turn is linearly proportional to the magnetic field and inversely proportional to the effective mass of the electron. Thus, due to the very small effective mass of the electron in an InSb dot the energy of the spinor 3 exceeds the energy of the spinor 2 already at very small magnetic fields. Consequently also the crossing of absorption lines of an InSb dot occurs at very small magnetic fields as can be seen in Figs. 5(b)–5(d).

At this point it may be worth mentioning that the energetics of the single-electron quantum dot under the influence of the SO coupling and subjected to an external magnetic field depends strongly on the sign of the Landé g factor. This is contrary to the case without the SO coupling where the energy spectrum is independent of the sign of g although, of course, the orientation of spin is determined by it. Let us consider, for example, the lowest absorption branch in the case $g > 0$. From Table I we can deduce that also in this case

the transitions mainly take the spinor 0 to the spinor 2. Now, however, there is no spinor level that would cross or even come close to the energy of the state 2 and mix with it. Consequently the anticrossing described above would not be observable in this case.

This concludes our discussion of the energy levels and optical-absorption spectra in a noninteracting QD in a magnetic field and in the presence of the SO interaction. In what follows, we describe the theory for an interacting few-electron parabolic quantum dot.

III. MANY-ELECTRON SYSTEMS

The basis $\mathcal{B}_N$ for N interacting electrons in a QD is constructed as a direct antisymmetrized product of single-particle bases $\mathcal{B}_S$ (27) of the form

$$
\begin{aligned}
\mathcal{B}_N &= \mathcal{A} \bigotimes_{j=1}^{N} \mathcal{B}_S \\
&= \{|\Lambda_i\rangle \,|\, i = 1, 2, \ldots\} \\
&= \{|\lambda_{i_1}; \lambda_{i_2}; \ldots; \lambda_{i_N}\rangle \,|\, i_j = 0, 1, 2, \ldots\} \\
&= \{|k_1, \ell_1; \ldots; k_N, \ell_N\rangle \,|\, k_j = 0, 1, \ldots; \ell_j = 0, \pm 1, \ldots\},
\end{aligned}
\tag{32}
$$

where $\mathcal{A}$ stands for the antisymmetrization operator. It is also understood that the notations such as $|\lambda_{i_1}; \lambda_{i_2}; \ldots; \lambda_{i_N}\rangle$ represent the antisymmetrized direct products, i.e.,

$$
|\Lambda_q\rangle = |\lambda_{i_1}; \lambda_{i_2}; \ldots; \lambda_{i_N}\rangle = \mathcal{A}[|\lambda_{i_1}\rangle \otimes |\lambda_{i_1}\rangle \otimes \cdots \otimes |\lambda_{i_1}\rangle].
\tag{33}
$$

Usually it is possible to restrict the size of $\mathcal{B}_N$ using the conservation laws. For example, in a rotationally invariant system the total angular momentum is a good quantum number. Therefore we fix it to J and accept into the basis only those states that satisfy

$$
\sum_{i=1}^{N} j_i = J.
$$

The states of the interacting system are expressed as a superposition of noninteracting states taken from the basis set (32)

$$
|\Psi\rangle = \sum_{i=1}^{\infty} c_i |\Lambda_i\rangle.
\tag{34}
$$

To extract the coefficients c_i, we again resort to minimization, i.e., we minimize the Rayleigh quotient

$$
\rho = \frac{\langle \Psi | \mathcal{H} | \Psi \rangle}{\langle \Psi | \Psi \rangle},
$$

where $\mathcal{H}$ is the total many-body Hamiltonian. Again this leads to the diagonalization of the Hamiltonian matrix with elements $\langle \Lambda_i | \mathcal{H} | \Lambda_j \rangle$. The eigenvectors are the desired expansion coefficients and the eigenvalues the corresponding energies of the interacting system. It will be clear from the Appendix that both these tasks, construction of the Hamil-

tonian matrix and its diagonalization, are numerically quite challenging.

A. Coulomb matrix elements

We write the total Hamiltonian $\mathcal{H}$ as a sum of the single-particle operators (4) and two-body operators $V(\vec{r}, \vec{r}')$ as

$$\mathcal{H} = \sum_{i=1}^{N} \mathcal{H}_0(\vec{r}_i) + \frac{1}{2} \sum_{i \neq j}^{N} V(\vec{r}_i, \vec{r}_j). \tag{35}$$

Since our basis states $|\Lambda_i\rangle$ are diagonal by construction in $\mathcal{H}_0$ we only need to evaluate the matrix elements of the latter sum in (35). Our many-body states $|\Lambda_i\rangle$ are expressed in occupation representation language (33), and therefore it is natural to proceed in the occupation number space. This means that for the interaction part we have to evaluate the two-body terms

$$V_{\lambda_1 \lambda_2 \lambda_3 \lambda_4} = \langle \lambda_1 \lambda_2 | V | \lambda_3 \lambda_4 \rangle. \tag{36}$$

In our system the mutual interaction between the electrons is taken to be purely Coulombic, i.e.,

$$V(\vec{r}, \vec{r}') = \frac{e^2}{\epsilon |\vec{r} - \vec{r}'|}, \tag{37}$$

where ϵ is the effective dielectric constant of the material. The interaction operator is thus diagonal in spin. Recalling that our single-particle states $|\lambda\rangle$ were two-component spinors (8), the two-body term (36) consists of a sum of four terms and is of the form

$$V_{\lambda_1 \lambda_2 \lambda_3 \lambda_4} = \sum_{\sigma, \sigma'} \int d\vec{r}\, d\vec{r}'\, \phi_1^{\sigma*}(\vec{r}) \phi_2^{\sigma'*}(\vec{r}') V(\vec{r}, \vec{r}') \phi_3^{\sigma'}(\vec{r}') \phi_4^{\sigma}(\vec{r})$$
$$\tag{38}$$

where the summation indices take values $\uparrow$ and $\downarrow$. Furthermore, since we expressed the spatial components ϕ^σ as superpositions of functions $g_{n\ell} e^{i\ell\theta}$ [Eq. (17)],

$$g^{\uparrow,\downarrow} = \sum_{n=0} c_{n,\ell}^{\uparrow,\downarrow} g_{n,\ell},$$

we are ultimately led to evaluate the Coulomb matrix elements in the oscillator wave function

$$w_{n\ell}(\vec{r}) = g_{n\ell} e^{i\ell\theta} = \sqrt{\frac{n!}{(n+|\ell|)!}} e^{-x/2} x^{|\ell|/2} L_n^{|\ell|}(x) e^{i\ell\theta}$$

basis. These matrix elements can be expressed in terms of finite sums as[4]

$$\mathcal{A}_{\ell_1 \ell_2 \ell_3 \ell_4}^{n_1 n_2 n_3 n_4} = \langle w_{n_1 \ell_1} w_{n_2 \ell_2} | \frac{e^2}{\epsilon |\vec{r} - \vec{r}'|} | w_{n_3 \ell_3} w_{n_4 \ell_4} \rangle = \delta_{\ell_1 + \ell_2, \ell_3 + \ell_4} \frac{\sqrt{2} e^2}{\epsilon a} \left(\frac{n_1!}{(n_1 + |\ell_1|)!} \right)^{1/2} \left(\frac{n_2!}{(n_2 + |\ell_2|)!} \right)^{1/2} \left(\frac{n_3!}{(n_3 + |\ell_3|)!} \right)^{1/2} \left(\frac{n_4!}{(n_4 + |\ell_4|)!} \right)^{1/2}$$

$$\times \sum_{\kappa_1=0}^{n_1} \sum_{\kappa_2=0}^{n_2} \sum_{\kappa_3=0}^{n_3} \sum_{\kappa_4=0}^{n_4} \left[\kappa_1 + \kappa_4 + \frac{1}{2}(|\ell_1| + |\ell_4| - k) \right]! \left[\kappa_2 + \kappa_3 + \frac{1}{2}(|\ell_2| + |\ell_3| - k) \right]!$$

$$\times \frac{(-1)^{\kappa_1 + \kappa_4}}{\kappa_1! \kappa_4!} \frac{(n_1 + |\ell_1|)!(n_4 + |\ell_4|)!}{(n_1 - \kappa_1)!(|\ell_1| + \kappa_1)!(n_4 - \kappa_4)!(|\ell_4| + \kappa_4)!} \frac{(-1)^{\kappa_2 + \kappa_3}}{\kappa_2! \kappa_3!} \frac{(n_2 + |\ell_2|)!(n_3 + |\ell_3|)!}{(n_2 - \kappa_2)!(|\ell_2| + \kappa_2)!(n_3 - \kappa_3)!(|\ell_3| + \kappa_3)!}$$

$$\times \sum_{s=0}^{\kappa_{14}} \frac{\left[\kappa_1 + \kappa_4 + \frac{1}{2}(|\ell_1| + |\ell_4| + k) \right]!}{\left[\kappa_1 + \kappa_4 + \frac{1}{2}(|\ell_1| + |\ell_4| - k) - s \right]!(k+s)!} \sum_{t=0}^{\kappa_{23}} \frac{\left[\kappa_2 + \kappa_3 + \frac{1}{2}(|\ell_2| + |\ell_3| + k) \right]!}{\left[\kappa_2 + \kappa_3 + \frac{1}{2}(|\ell_2| + |\ell_3| - k) - t \right]!(k+t)!}$$

$$\times \frac{(-1)^{s+t}}{s! t!} \frac{\Gamma\left(k + s + t + \frac{1}{2} \right)}{2^{k+s+t+1}}, \tag{39}$$

where $\kappa_{14} = \kappa_1 + \kappa_4 + \frac{1}{2}(|\ell_1| + |\ell_4| - k)$, $\kappa_{23} = \kappa_2 + \kappa_3 + \frac{1}{2}(|\ell_2| + |\ell_3| - k)$, and $k = |\ell_1 - \ell_4| = |\ell_2 - \ell_3|$. Numerical techniques to evaluate these two-body terms and to diagonalize the resulting Hamiltonian matrix are described in the Appendix.

IV. RESULTS AND DISCUSSION

For numerical evaluation of the energy spectra and the optical-absorption spectra for QDs with a few interacting electrons, we have considered the InAs, InSb, and GaAs quantum dots. Parameters of these systems are already given in Sec. II. The energy spectra and the optical-absorption spectra for these three systems are described in the subsections below.
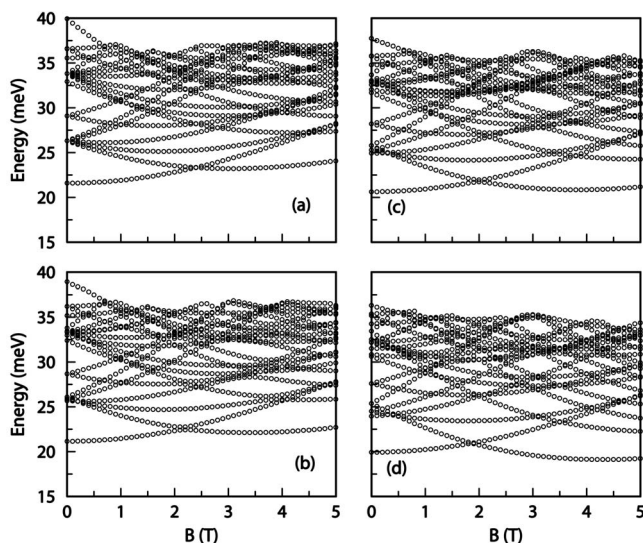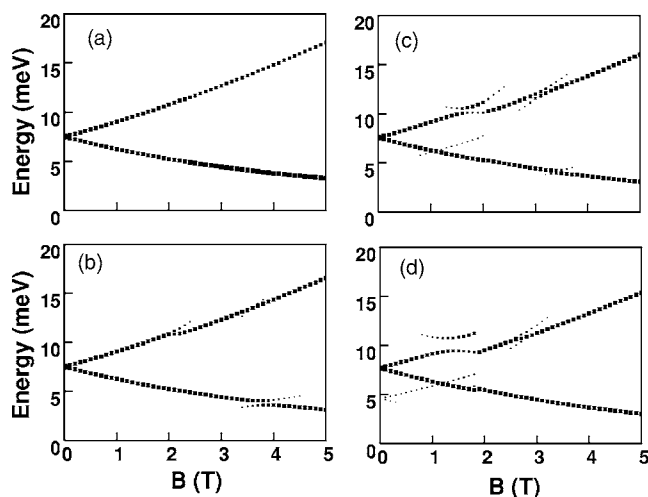
FIG. 7. Some of the low-lying energy states for two interacting electrons confined in an InAs quantum dot and for various values of the SO coupling strength (in meV nm) $\alpha=$(a) 0, (b) 20, (c) 30, and (d) 40.

A. InAs quantum dots

Our numerical results for energy spectra and absorption spectra (dipole allowed) for 2–4 electrons are presented in Figs. 7–12 and for various values of the SO coupling strength (in meV nm) α. We have considered the parameters for the InAs quantum dot as listed in Sec. II B. Results for a lower confinement energy $\hbar\omega_0=3.75$ meV are available in our earlier report.[11]

A striking feature visible in the absorption spectra (Figs. 8, 10, and 12) is the appearance of discontinuities, anticrossings, and new modes in addition to the two main ($\alpha=0$) absorption lines. These optical signatures of the SO interac-

FIG. 8. Dipole-allowed transition energies for two interacting electrons confined in an InAs quantum dot and for various values of the SO coupling strength (in meV nm) $\alpha=$(a) 0, (b) 20, (c) 30, and (d) 40. The size of the points in the figures is proportional to the calculated intensity.
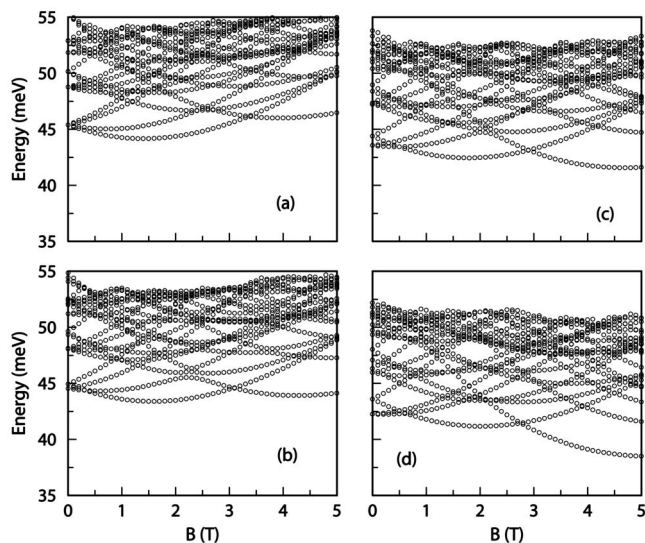
FIG. 9. Same as in Fig. 7 but for a three-electron InAs quantum dot.

tion are consequences of the multitude of level crossings and level repulsions that occur in the energy spectra (Figs. 7, 9, and 11). The latter can be attributed to an interplay between the SO and Zeeman couplings. In order to understand their origin, let us first examine the case of the two-electron system (Figs. 7 and 8). In our spinor notation the main contribution to the ground state at zero magnetic field comes from the two-electron state $|\lambda_{\ell_1},\lambda_{\ell_2}\rangle=|\lambda_0,\lambda_{-1}\rangle$, where $|\lambda_{\ell_1}\rangle$ is a spinor with $j_1=\ell_1+1/2=1/2$, $d_n^{\lambda_1}=0$, and $|\lambda_{\ell_2}\rangle$ a spinor with $j_2=-1/2$ and $u_n^{\lambda_2}=0$, i.e., both electrons have zero orbital angular momenta with opposite spins (corresponding to the spinors 0 and 1 in Table I with $J=j_1+j_2=0$). When we increase the magnetic field the spin triplet configuration will become, due to the interaction, energetically more favorable. If the Land'e g factor is negative then the electrons would like to occupy states with orbital angular momenta 0 and -1 with both spins up (i.e., states 0 and 2 of Table I). In the
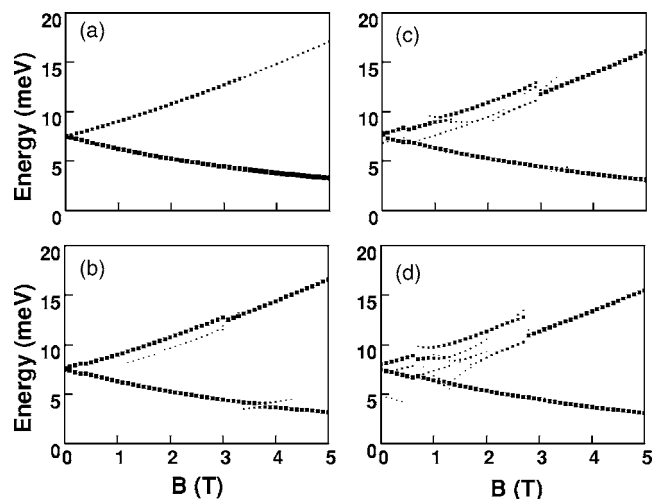

FIG. 10. Same as in Fig. 8, but for a three-electron InAs quantum dot.
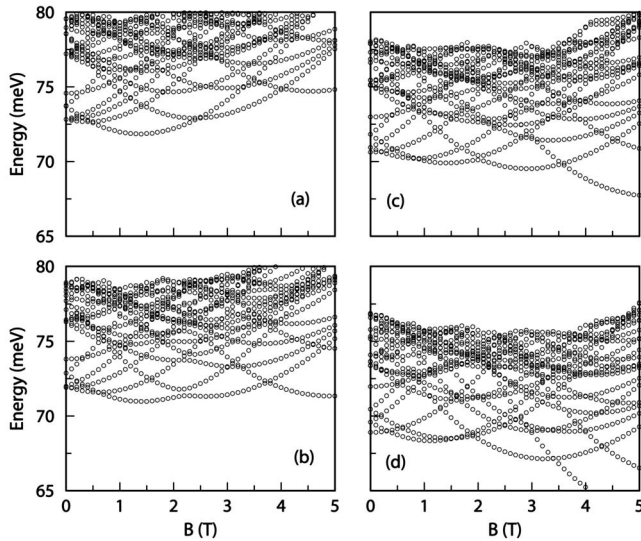
FIG. 11. Same as in Fig. 7 but for a four-electron InAs quantum dot.

spinor picture this means that $|\lambda_{\ell_2}\rangle$ still has $\ell_2 = -1$ ($J=0$) but now $u_n^{\lambda_2} \neq 0$ and $d_n^{\lambda_2} = 0$. The SO interaction mixes these two configurations which results in a level repulsion. On the other hand, when the strength of the SO coupling is further increased, the relative significance of the Zeeman contribution to $\mathcal{H}_0$ decreases. The energy shifts to states with $J \neq 0$ will then become energetically feasible and we again have crossings of levels. For increasing number of electrons in the dot, the energy spectra are more dense and exhibit additional level crossings (Figs. 9–12). As a consequence, the ground-state angular momentum also changes more frequently as compared to that of the two-electron case. It should be pointed out that in many-electron dots these level crossings and repulsion are to be attributed, at least partly, to the mutual Coulomb interactions. The level crossings and repulsions we saw earlier [e.g., levels 1 and 2 in Fig. 1(a)] in the single-particle picture are due to the Zeeman splitting whereas in interacting systems crossings occur even in the
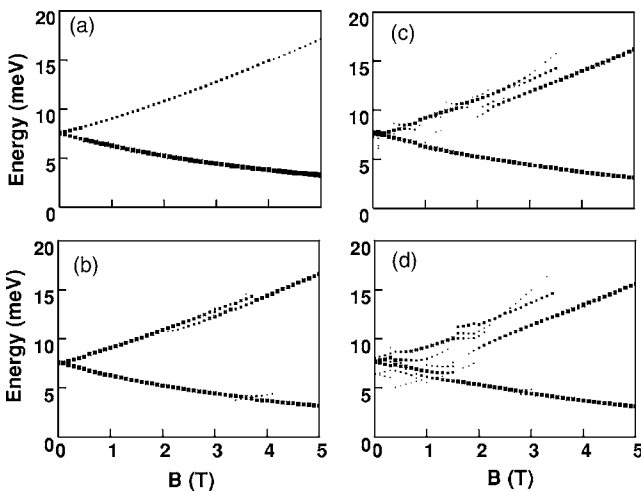

FIG. 12. Same as in Fig. 8, but for a four-electron InAs quantum dot.

limit of vanishing Zeeman coupling. In the present InAs dot the Coulomb interaction brings, for example, the singlet-triplet transition to much lower magnetic field ($B \approx 2$ T) as compared to the field required in a noninteracting system ($B \approx 4$ T).

At moderate SO coupling strengths the absorption spectra do not essentially differ from the single-particle spectrum. But when the coupling strength increases the deviation from the pure parabolic confinement also increases, which in turn implies that the lowest final states of dipole-allowed transitions are no longer achievable by adding $\hbar\Omega \pm \frac{1}{2}\hbar\omega_c$ to the initial-state energies. In particular, this results in discontinuities and anticrossings as well as appearance of new modes. As an illustration, let us consider the absorptions that at a magnetic field of $B=1$ T take the two-electron system from the ground state to excited states. In the absence of the SO coupling the ground state is a spin-singlet state $S=0$ with total angular momentum $J=0$. According to the dipole selection rules absorptions cause transitions to states $J=\pm 1$ and $S=0$ with energies $\Delta E_\pm$ above the ground state. In Fig. 8(d), we note that in addition to the two main lines there are now two additional lines (at around $B=1$ T) of appreciable intensity at the SO coupling strength $\alpha=40$ meV nm. Further analysis reveals that the ground states still have $J=0$ and that the expectation value of the spin z component is $\langle \sigma_z \rangle = 0$. The excited states also have $J=\pm 1$, as before. However, the final spin states can no longer be classified as singlets: the expectation values $\langle \sigma_z \rangle$ vary between -0.03 and 0.39. When the number of electrons increases the number of these additional modes also increases but at the same time the relative intensities decrease (at each B we have normalized the total intensity to unity). On the other hand, the discontinuities as consequences of deviations from a parabolic confinement become more pronounced (Figs. 9–12). This is because there are higher angular momenta involved in the dipole transitions. As a consequence of this the upper absorption branch now exhibits a rich structure while in the single-particle picture it is practically featureless.

B. InSb quantum dots

As mentioned above, in addition to the InAs quantum dots, investigation of InSb quantum dots is also thought to be interesting, particularly in the context of SO coupling effects due to the large values of $|g|$ and α.[45] We have considered the parameters for the InSb quantum dot that can be found in Sec. II B. The energy levels for InSb quantum dots containing 2–4 interacting electrons for various values of the SO coupling strength α, and the corresponding optical-absorption spectra, are presented in Figs. 13–18. As compared to the spectra of InAs dots a clear difference is the almost total absence of anticrossings and discontinuities. This is partly due to the very large Zeeman coupling which practically nullifies the SO interaction at the coupling strengths α we are concerned with. Another reason is the large kinetic energies due to the very small electron effective mass. Because the strength of the Coulomb interaction is somewhat smaller than in InAs ($\epsilon_{InSb} > \epsilon_{InAs}$) correlations caused by the mutual electronic interactions are effectively

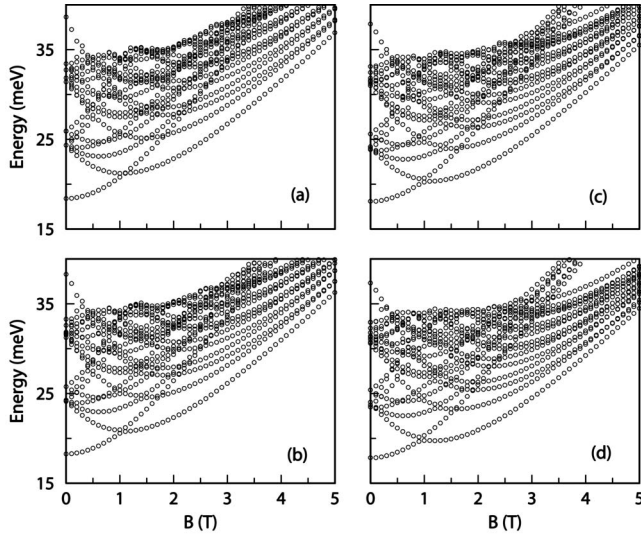FIG. 13. Same as in Fig. 7 but for a two-electron InSb quantum dot.

FIG. 15. Same as in Fig. 7 but for a three-electron InSb quantum dot.

much smaller in InSb than in InAs. For the exploration of SO coupling via absorption spectroscopy, InSb quantum dots do not seem to be a very promising system.

C. GaAs quantum dots

The results for GaAs quantum dots, ones that are most intensely explored in the absence of SO coupling, are presented here primarily for academic interest. Again, the parameters that we have used here are already listed in Sec. II B. Clearly, the very low value of the $|g|$ factor perhaps makes the GaAs QDs unsuitable for any observable effect due to the SO coupling. Interestingly, however, among all the three types of QDs studied here for optical absorption, GaAs QDs show the most spectacular effects for large values of α. The energy levels for GaAs quantum dots containing 2–4 interacting electrons for various values of the SO coupling strength α, and the corresponding optical-absorption spectra,
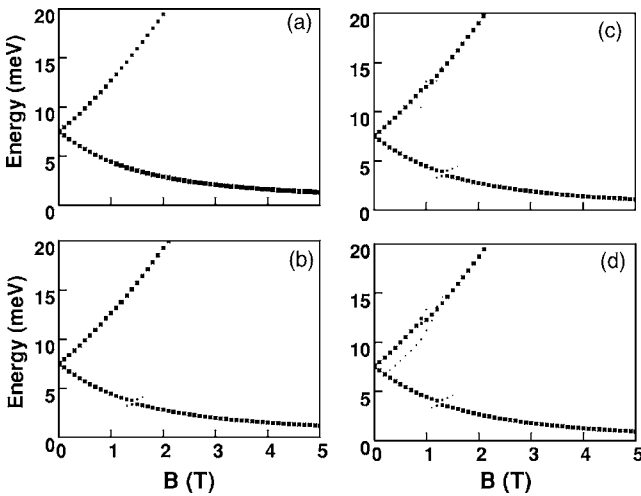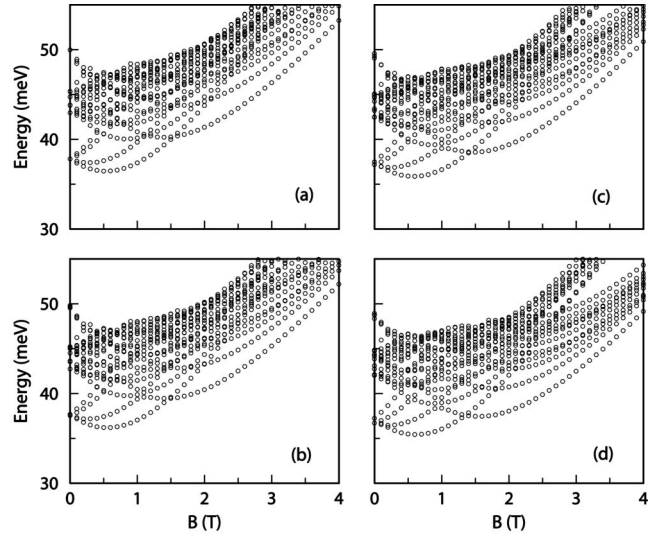
are presented in Figs. 19–24. As mentioned above, the only observed value of α for GaAs QD reported as yet is $\alpha \sim 6$ meV nm.[28] Reversing the arguments presented in the previous subsection, i.e., in GaAs a very small Zeeman coupling and a rather large effective electron mass but practically equal strength of Coulomb interaction, help us understand why the absorption spectra of our GaAs dots exhibit a remarkably rich structure as opposed to those of the InSb and InAs dots. Finding an appropriate setup to generate a large α for GaAs quantum dots would be a major (but worthwhile) experimental endeavor.

V. A BRIEF REVIEW OF EARLIER THEORETICAL WORK

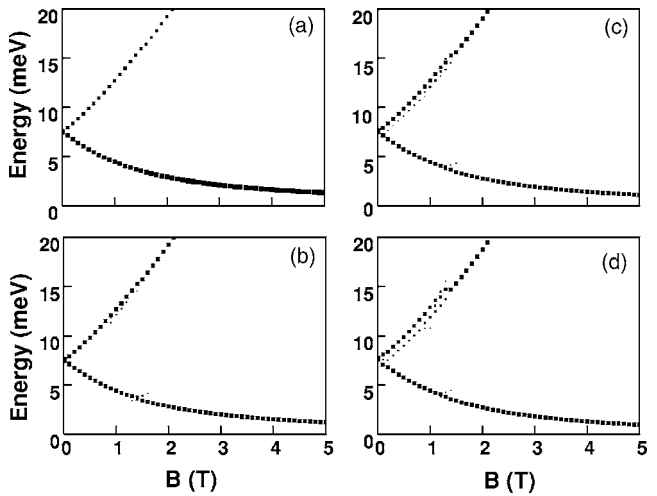In this section, we present a critical review of earlier theoretical reports on how the Bychkov-Rashba spin-orbit cou-

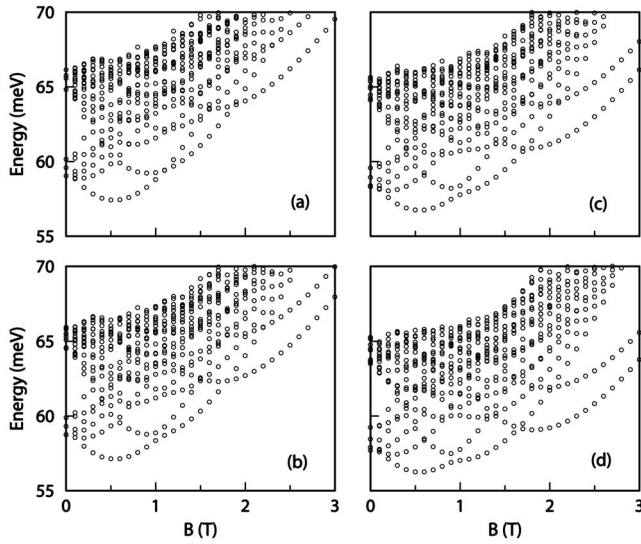FIG. 14. Same as in Fig. 8, but for a two-electron InSb quantum dot.

FIG. 16. Same as in Fig. 8, but for a three-electron InSb quantum dot.

FIG. 17. Same as in Fig. 7 but for a four-electron InSb quantum dot.

FIG. 19. Same as in Fig. 7 but for a two-electron GaAs quantum dot.

pling in parabolic quantum dots was treated.[14–30] There are quasiexact solutions available for electrons confined in a parabolic quantum dot in the presence of the SO interaction, but without the interelectron interaction,[19] and exact analytical results are also reported in the case of a circular quantum dot with hard walls,[20] again for a noninteracting system, but with the Bychkov-Rashba spin-orbit interaction included. However, for realistic systems of parabolic quantum dots with interacting electrons these methods are prohibitively complicated and evaluation of the energy spectrum can only be done numerically. Among the theoretical papers dealing with the SO interaction in quantum dots discussed below, Kuan *et al.*[14] presented the best treatment of the single-electron states. They looked at the energy levels of parabolically confined quantum dots with Bychkov-Rashba SO coupling and in the presence of zero and nonzero magnetic fields. They solved the single-particle equation correctly by expanding the solution spinors in terms of the eigenfunctions
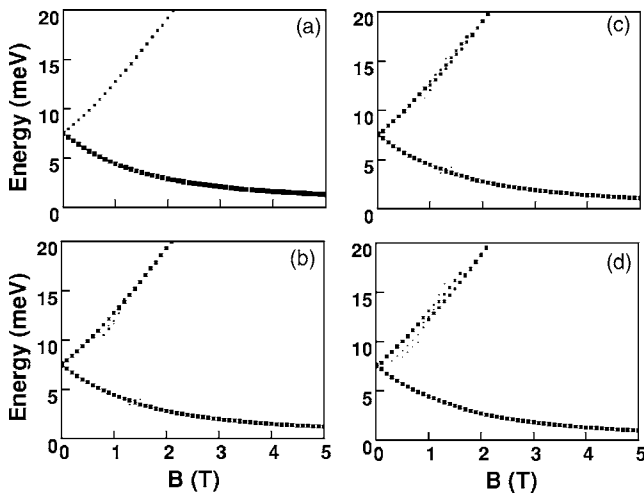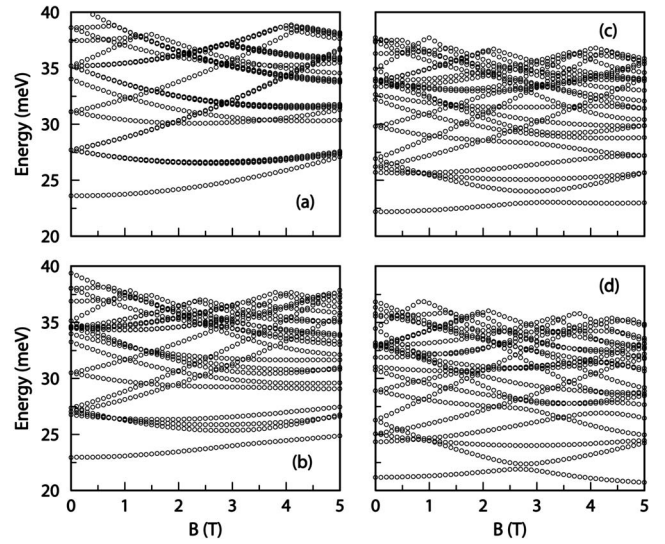
of QDs without the SO interaction, i.e., the Laguerre functions. We have used a similar approach to construct the basis states for our multielectron QDs (Secs. II and III).

Voskoboynikov *et al.*[15] studied the effect of the SO interaction on the energy spectrum of cylindrical semiconductor QDs in an externally applied magnetic field. They considered the Bychkov-Rashba SO coupling due to the parabolic confinement, i.e., an in-plane field conserving orbital and spin angular momenta. As a consequence, the SO coupling has no qualitative effects on, for example, the absorption spectra. The electron-electron interaction was not included in this scheme. In Ref. 16, they studied the magnetization and magnetic susceptibility in few-electron parabolic QDs with the SO coupling. As in their earlier paper, they handled the SO term only due to the parabolic confinement and therefore the single-particle Hamiltonian is diagonal in spin space. They neglected the mutual electronic Coulomb interaction.

Governale[17] investigated the effects of the SO coupling on the addition energy and on the spin properties of few-
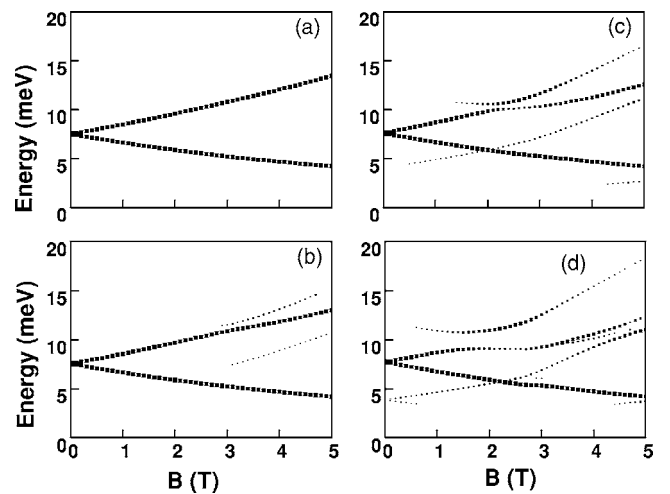

FIG. 18. Same as in Fig. 8, but for a four-electron InSb quantum dot.

FIG. 20. Same as in Fig. 8, but for a two-electron GaAs quantum dot.

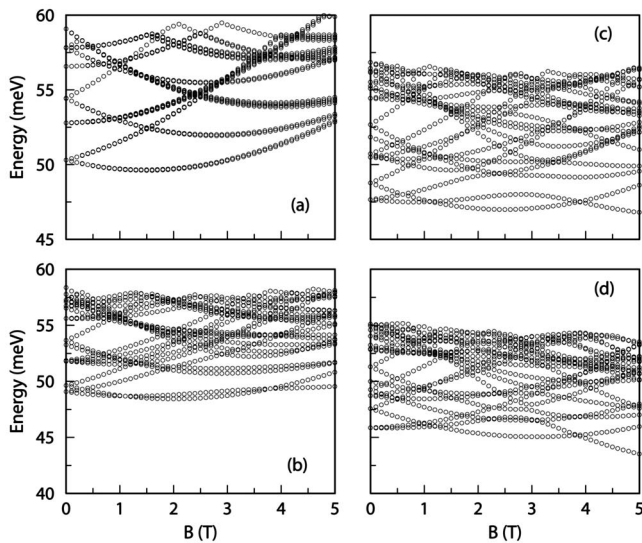FIG. 21. Same as in Fig. 7 but for a three-electron GaAs quantum dot.

FIG. 23. Same as in Fig. 7 but for a four-electron GaAs quantum dot.

electron QDs in the absence of an external magnetic field. He introduced the SO coupling into single-particle states perturbatively but also compared the resulting energies to the ones obtained by the numerical diagonalization technique. At the small SO coupling strength that he considered, the perturbation approach seems to be valid. Electron correlations were handled by using the spin-density functional approach. Cremers et al.[18] studied conductance and its fluctuations in the presence of the SO interaction, Zeeman coupling, and an externally applied magnetic field, in a (single-electron) QD. They solved the single-particle equation by applying an approximate unitary transformation which in leading order takes the Hamiltonian to a diagonal form in spin space.

Valin-Rodriguez[21] considered a single electron in a parabolic QD with Bychkov-Rashba SO coupling. He performed a unitary transformation to transform the Hamiltonian in spin space to a diagonal form up to second order in SO and Zeeman coupling parameters. He showed that the effective SO
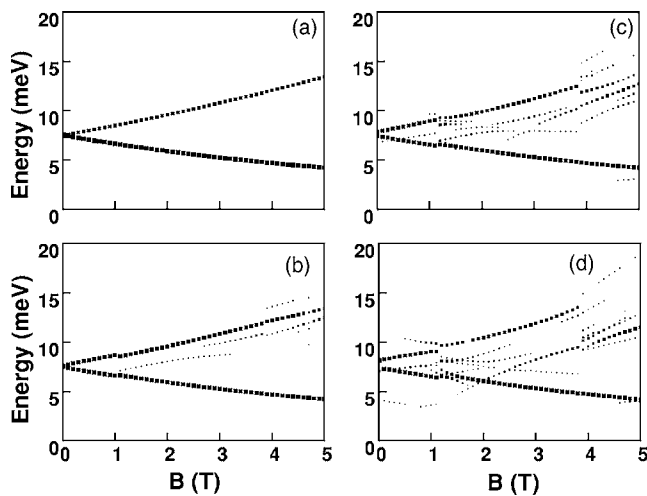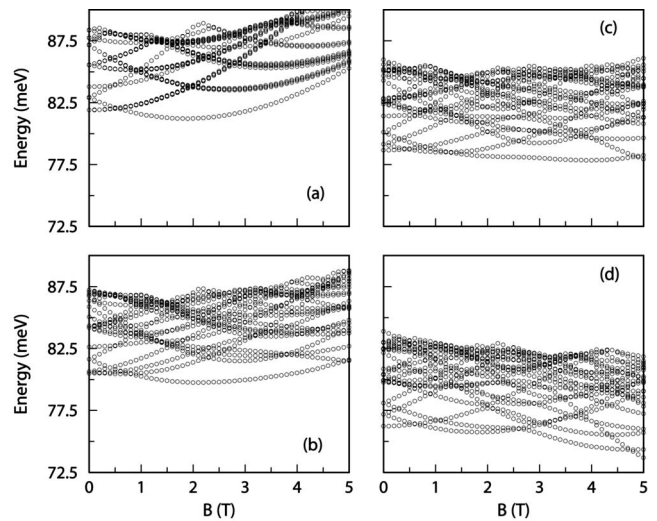
interaction is influenced by the interplay between Zeeman and SO couplings. In Ref. 22, Valin-Rodriguez et al. introduced a spatially modulated (in the radial direction) Bychkov-Rashba coupling in single-electron (disk) QDs. They solved the two-component spinor equation and numerically evaluated the spin density. They concluded that it is possible to confine electrons spatially with appropriate structural modulation. These authors also investigated the SO couplings in deformed parabolic quantum dots.[23] They solved the single-particle equations using the approximate unitary transformations mentioned above. They were interested in the effects of spatial deformations on the spin splitting oscillations. They estimated the Coulomb interaction contribution using the time-dependent local-spin-density approximation.[24]

Lucignano et al.[25] studied few-electron QDs including the mutual electron-electron interaction and under the influence of an externally applied magnetic field. They applied an exact diagonalization method (but with a rather restricted basis:
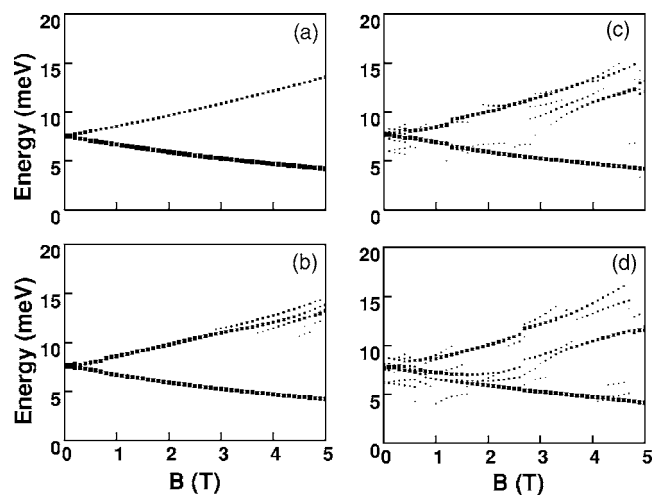

FIG. 22. Same as in Fig. 8, but for a three-electron GaAs quantum dot.

FIG. 24. Same as in Fig. 8, but for a four-electron GaAs quantum dot.

28 single-particle states deducing from their earlier paper[46]). They particularly looked at the possibility of using the SO coupling to control the excitations under magnetic fields that polarize the ground state, i.e., close to the final *single-triplet* transition. The SO coupling is included in the many-electron Hamiltonian, but not in the basis states. They evaluated the dipole matrix elements for absorption from the ground state to the lowest dipole-allowed excited state. They claimed that there is an increase in intensity close to the transition to the fully polarized ground state.

Destefani *et al.*[26] reported numerical results for energy levels and spin polarizations for one- and two-electron parabolic QDs under a magnetic field and with SO coupling. For the two-electron system, Coulomb interaction was also included. They constructed single-electron states approximately in the two-electron QD, however: the SO coupling was in fact taken into account only in the many-electron Hamiltonian, but not in the single-particle term. The SO coupling being a single-particle effect, this omission will affect the accuracy of their numerical results. Debald *et al.*[27] studied oscillations in few-electron parabolic QDs in a magnetic field, between states where the degeneracy is lifted by the SO coupling, i.e., at the level repulsion points. The Coulomb interaction was taken into account only approximately, because the many-body effects were claimed to play only a minor role in the very small magnetic field considered in that work. Könemann *et al.*[28] considered the SO coupling in single-electron QDs. They showed that there is an anisotropy between spin splittings due to magnetic fields parallel and perpendicular to the dot. The anisotropy was shown to be proportional to the strength of the SO coupling. Bellucci and Onorato[29] studied the influence of the SO coupling on the charge and spin polarization in a vertical disk-shaped QD under a strong perpendicular magnetic field. They treated the SO coupling perturbatively (up to second order). They handled the Coulomb interaction within the Hartree-Fock approach. They studied the energy splittings due to the SO coupling. Finally, Fransson *et al.*[30] studied transport through QDs with spin-dependent couplings to the contacts. They evaluated the QD energy levels using a (first-principles) density functional theory. They calculated the transport properties of (a) noninteracting electrons taking into account the few levels closest to the Fermi level, and (b) interacting electrons using an approximate Hamiltonian with the levels closest to the Fermi level.

We would like to note here that, in the light of all these theoretical approaches, our method of including the SO coupling for interacting electrons in a parabolic QD seems to be the most accurate one in the sense that in our approach, both the SO interaction and mutual Coulomb interactions are treated exactly. However, given the fact that our approach involves extensive numerical computations, some of the other approaches discussed above, such as the one by Lucignano *et al.*,[25] seem to be very promising.

VI. CONCLUSIONS

In conclusion, we have studied the energy levels and optical-absorption spectra for parabolic quantum dots con-

taining up to four interacting electrons, in the presence of spin-orbit coupling and under the influence of an externally applied perpendicular magnetic field. We have presented a very accurate numerical scheme to evaluate these quantities. We have presented results for the Fock-Darwin spectra in the presence of the SO coupling for quantum dots made out of three different semiconductor systems, InAs, InSb, and GaAs. The effects of the SO coupling on the single-electron spectra are primarily to lift the degeneracy at $B=0$, rearrangement of some of the energy levels at small magnetic fields, and level repulsions at high fields. These effects are explained as due to mixing of different spinor states for increasing strength of the SO coupling. As a consequence, the corresponding absorption spectra reveal anticrossing structures in the two main lines ($\alpha=0$) of the spectra. For interacting many-electron systems we observed the appearance of discontinuities, anticrossings, and new modes that appear in conjunction with the two main absorption lines. These additional features arise entirely due to the SO coupling and are a consequence of level crossings and level repulsions in the energy spectra. An intricate interplay between the SO coupling and the Zeeman energies is shown to be responsible for these additional features seen in the energy spectra. Our accurate results for the low-lying energy levels for the SO coupled QDs can also be measured, in principle, by transport[40] or capacitance[41] spectroscopy, which have been successfully employed earlier to map out the energy spectra of parabolic quantum dots. Optical-absorption spectra for all three types of quantum dots containing a few interacting electrons that are studied here show a common feature: additional modes appear, mostly near the upper main branch of the spectra around 2 T, that become stronger with increasing α. Among the three types of systems considered here, the optical signature of the SO interaction is found to be the strongest in the absorption spectra of a GaAs quantum dot, but only at very large values of the SO coupling strength, and appears to be the weakest for the InSb quantum dots. Experimental observation of these optical modes that appear solely due to the presence of the SO coupling would be very exciting because that would be a major step forward in our quest to manipulate the spin dynamics in nanostructured systems via the SO coupling.

Our future work along this line will be to explore coupled QDs, or QD molecules.[47] Our primary goal will be to generate accurate results for energy levels and optical-absorption spectra for coupled (laterally[48] or vertically[49]) quantum dots with spin-orbit interaction. In addition to being important for fundamental studies, these results would be interesting from the point of view of quantum computations[50] as well. It is now well recognized that semiconductor quantum dots have the potential to become the building blocks for solid state quantum computation. Quantum states of single-, double-, and even triple-coupled[51] quantum dots have been explored for this purpose. In a quantum computer, information is stored in a two-level system. Hence a promising candidate system to realize the quantum bit, the fundamental unit of information in a quantum computer, is a quantum dot where the single-electron states can be used for that purpose. In a magnetic field, the Zeeman splitting of electron spin can provide a two-level system (for an odd number of electrons).

Alternatively, the spatial wave function of a single-electron state in a double quantum dot (allowing for electron tunneling between the two dots) can also represent a two-level system. Spin-orbit coupling in coupled-quantum-dot systems could perhaps be used to perform quantum computation (using the spin rotation, for example). Accurate results for the energy levels of the coupled-dot system might be beneficial in that direction of research. The effects of the SO coupling on the energy levels and absorption spectra for a more complex system such as coupled QDs are, however, important and interesting in their own ways. These will be the subjects of our future research.

APPENDIX: DIAGONALIZATION OF MONSTER MATRICES

We have mentioned in Sec. III the challenging task of construction of the Hamiltonian matrix and its numerical diagonalization. Here we present a brief discussion about the numerical method that we believe the most accurate (and appropriate) for that task. While in principle, evaluation of Eq. (39) is straightforward it turns out to be numerically highly unstable, primarily due to the expansion (17) extending to Laguerre polynomials of large degree and large angular momenta which in turn, leads to large terms of alternating sign.[52] A remedy for this is to employ multiple precision arithmetics such as, for example, implemented in the GNU arbitrary precision GMP library. However, if we apply multiple precision arithmetic directly into the sixfold summation (39) the time consumed to evaluate these terms becomes insurmountable. To circumvent this obstacle we note that many terms in the sums actually depend on very few parameters, the range of these parameters is restricted, and the same functional forms repeat themselves. Thus a natural solution is to tabulate these forms and the subsums. In our Coulomb matrix element code we used the tabulated functions

$$D(i) = i!,$$

$$F(n,\ell,\kappa) = \frac{(n+\ell)!}{(n-\kappa)!(\ell+\kappa)!} = \frac{D(n+\ell)}{D(n-\kappa)D(\ell+\kappa)},$$

$$G(n,\ell,\kappa) = \frac{(n+\ell)!}{\kappa!(n-\kappa)!(\ell+\kappa)!} = \frac{F(n+\ell)}{D(\kappa)},$$

$$H(s) = \frac{\Gamma\left(s+\frac{1}{2}\right)}{2^{s+1}},$$

$$I(q_1,q_2,\ell) = D(q_1)D(q_2)\sum_{s=0}^{q_1}(-1)^s G(q_1,\ell,s)$$

$$\times \sum_{t=0}^{q_2}(-1)^t G(q_2,\ell,t)H(t+s+\ell).$$

Now the summations Σ in the expression (39) can be written as

$$\Sigma = \sum_{\kappa_1=0}^{n_1}(-1)^{\kappa_1}G(n_1,\ell_1,\kappa_1)\sum_{\kappa_2=0}^{n_2}(-1)^{\kappa_2}G(n_2,\ell_2,\kappa_2)$$

$$\times \sum_{\kappa_3=0}^{n_3}(-1)^{\kappa_3}G(n_3,\ell_3,\kappa_3)\sum_{\kappa_4=0}^{n_4}(-1)^{\kappa_4}G(n_4,\ell_4,\kappa_4)$$

$$\times I\left[\kappa_1+\kappa_4+\frac{1}{2}(\ell_1+\ell_4-k),\kappa_2+\kappa_3\right.$$

$$\left.+\frac{1}{2}(\ell_2+\ell_3-k)\right]. \tag{A1}$$

Although the summation here is still fourfold it is nevertheless several orders of magnitude faster than the original one (39) and as such fast enough for our purposes.

Under the influence of the SO coupling the total spin S of our many-electron system is not a conserved quantity. As a consequence of this we cannot fix the total S_z of the many-body basis. This degree of freedom tends to make the number of noninteracting many-body states of the basis very large even for a small number of electrons, and even if the conservation of the total angular momentum $J_z=L+S_z$ is taken into account. For example, to achieve a convergence for a four-electron system in the parabolic confinement with harmonic potential ($\hbar\omega_0$) of a few meV the size of the basis must be of the order of a million. Furthermore, since we want to study properties of the eigenstates, such as polarization and dipole matrix elements between states, we also need the relevant eigenvectors. Clearly the sheer size of the matrix prohibits a full diagonalization and we have to resort to an iterative scheme aimed to search for a given number of energetically lowest eigenvectors. Of course the algorithm should be fast and hopefully also robust.

The algorithm proposed by Davidson and Liu (DL) to evaluate the eigenvalues and eigenvectors of "monster matrices"[53] seems to fit our criteria. Like any other iterative method it transforms the diagonalization of a matrix A to minimization of the Rayleigh quotient

$$\lambda = \frac{x^T A x}{x^T x}, \tag{A2}$$

where x represents the column vector of the coefficients in the superposition of the basis states. Also, as in many other methods, the only operations involving the matrix A are vector multiplications. This allows us to exploit fully the sparseness of A, i.e., we have to store only the nonzero elements.

The key idea behind practically any iterative method subjecting the matrix only to multiplication is to search for the minimum of the quotient (A2) in a (very small) subspace and to update this subspace in each iteration step. How this updating is performed depends on the method. For example, in

the common conjugate gradient method the subspace is two-dimensional and spanned by the gradient g at current position x and a vector s conjugate to it with respect to A (i.e., $s^T A g = 0$).

In the DL method the dimension of the search space varies from step to step. Suppose that at a given step our search space $\mathcal{S}$ is spanned by the orthonormal vectors $s_1, \ldots, s_K$ (the dimension K must, of course, be greater than the number of required eigenstates). Finding the minimum of (A2) in this subspace corresponds to the diagonalization of the $K \times K$ matrix $\mathcal{S}^T A \mathcal{S}$ (we take $\mathcal{S}$ to represent also the matrix with columns s_k). As a result we get K eigenvalues μ_k and K eigenvectors z_k, each of dimension K. The expanded vectors

$$y_k = \sum_{i=1}^{K} z_{k,i} s_i$$

will approximate the eigenvectors and the quantities μ_k the

eigenvalues we are seeking. The next task in the iteration step is to update the subspace $\mathcal{S}$. For that purpose we pick up a certain number (a parameter depending, for example, on the size of the computer memory) of the residuals

$$r_k = (A - \mu_k) y_k$$

with largest norms. The selected residuals are orthonormalized with respect to the space $\mathcal{S}$ and then appended to it. So, in each step the dimension of the search space and the size required to store it increases and we may eventually exhaust all the memory. At this point we compress the space $\mathcal{S}$ to its bare minimum comprising only as many vectors as we are required to find. These vectors are selected from the set $\{y_k\}$ and are the ones with smallest μ_k.

---

*Electronic address: tapash@physics.umanitoba.ca

[1] *Nano-Physics & Bio-Electronics: A New Odyssey*, edited by T. Chakraborty, F. Peeters, and U. Sivan (Elsevier, Amsterdam, 2002).

[2] P. A. Maksym and T. Chakraborty, Phys. Rev. Lett. **65**, 108 (1990).

[3] T. Chakraborty, Comments Condens. Matter Phys. **16**, 35 (1992); V. Gudmundsson, A. Manolescu, R. Krahne, and D. Heitmann, in *Nano-Physics & Bio-Electronics: A New Odyssey* (Ref. 1), Chap. 7.

[4] T. Chakraborty, *Quantum Dots* (North-Holland, Amsterdam, 1999).

[5] C. Sikorski and U. Merkt, Phys. Rev. Lett. **62**, 2164 (1989).

[6] See, for example, I. Magnusdottir and V. Gudmundsson, Phys. Rev. B **60**, 16591 (1999); R. Krahne, V. Gudmundsson, C. Heyn, and D. Heitmann, *ibid.* **63**, 195303 (2001); E. Lipparini, N. Barberan, M. Barranco, M. Pi, and Ll. Serra, *ibid.* **56**, 12375 (1997); P. A. Maksym, Physica B **184**, 385 (1993); T. Seki, Y. Kuramoto, and T. Nishino, J. Phys. Soc. Jpn. **65**, 3945 (1996); M. Wagner, A. V. Chaplik, and U. Merkt, *ibid.* **51**, 13817 (1995); B. Meurer, D. Heitmann, and K. Ploog, Phys. Rev. Lett. **68**, 1371 (1992); T. Chakraborty, V. Halonen, and P. Pietiläinen, Phys. Rev. B **43**, 14289 (1991).

[7] D. Mowbray and J. Finley, in *Nano-Physics & Bio-Electronics: A New Odyssey*, Ref. 1, Chap. 3; M. S. Skolnick and D. J. Mowbray, Physica E (Amsterdam) **21**, 155 (2004).

[8] A. J. Shields, R. M. Stevenson, R. M. Thompson, Z. Yuan, and B. E. Kardynal, in *Nano-Physics & Bio-Electronics: A New Odyssey*, Ref. 1, Chap. 4.

[9] V. Fock, Z. Phys. **47**, 446 (1928); C. G. Darwin, Proc. Cambridge Philos. Soc. **27**, 86 (1930).

[10] For a similar result in a parabolic quantum well, see L. Brey, N. F. Johnson, and B. I. Halperin, Phys. Rev. B **40**, 10647 (1989).

[11] T. Chakraborty and P. Pietiläinen, Phys. Rev. Lett. **95**, 136603 (2005).

[12] *Semiconductor Spintronics and Quantum Computation*, edited by D. D. Awschalom, D. Loss, and N. Samarth (Springer, Berlin, 2002); D. Grundler, Phys. World **15**(4), 39 (2002); S. A. Wolf, D. D. Awschalom, R. A. Buhrman, J. M. Daughton, S. von Molnar, M. L. Roukes, A. Y. Chtchelkanova, and D. M. Treger, Science **294**, 1488 (2001); G. A. Prinz, Phys. Today **48**(4), 58 (1995).

[13] *Proceedings of the First International Conference on the Physics and Applications of Spin Related Phenomena in Semiconductors*, edited by H. Ohno [Physica E (Amsterdam) 10, (2001)]; G. Schmidt, C. Gould, and L. W. Molenkamp, *ibid.* **25**, 150 (2004).

[14] W. H. Kuan, C. S. Tang, and W. Xu, J. Appl. Phys. **95**, 6368 (2004).

[15] O. Voskoboynikov, C. P. Lee, and O. Tretyak, Phys. Rev. B **63**, 165306 (2001).

[16] O. Voskoboynikov, O. Bauga, C. P. Lee, and O. Tretyak, J. Appl. Phys. **94**, 5891 (2003).

[17] M. Governale, Phys. Rev. Lett. **89**, 206802 (2002).

[18] J. H. Cremers, P. W. Brouwer, and V. I. Falko, Phys. Rev. B **68**, 125329 (2003).

[19] H. Tütüncüler, R. Koc, and E. Olgar, J. Phys. A **37**, 11431 (2004).

[20] E. Tsitsishvili, G. S. Lozano, and A. O. Gogolin, Phys. Rev. B **70**, 115316 (2004).

[21] M. Valin-Rodriguez, Phys. Rev. B **70**, 033306 (2004).

[22] M. Valin-Rodriguez, A. Puente, and L. Serra, Phys. Rev. B **69**, 153308 (2004).

[23] M. Valin-Rodriguez, A. Puente, and L. Serra, Phys. Rev. B **69**, 085306 (2004).

[24] M. Valin-Rodriguez, A. Puente, L. Serra, and E. Lipparini, Phys. Rev. B **66**, 165302 (2002).

[25] P. Lucignano, B. Jouault, A. Tagliacozzo, and B. L. Altshuler, Phys. Rev. B **71**, 121310(R) (2005); P. Lucignano, B. Jouault, and A. Tagliacozzo, *ibid.* **69**, 045314 (2004).

[26] C. F. Destefani, S. E. Ulloa, and G. E. Marques, Phys. Rev. B **69**, 125302 (2004); **70**, 205315 (2004).

[27] S. Debald and C. Emary, Phys. Rev. Lett. **94**, 226803 (2005).

[28] J. Könemann, R. J. Haug, D. K. Maude, V. I. Falko, and B. L. Altshuler, Phys. Rev. Lett. **94**, 226404 (2005).

[29] S. Bellucci and P. Onorato, Phys. Rev. B **72**, 045345 (2005).

[30] J. Fransson, E. Holmström, O. Eriksson, and I. Sandalov, Phys. Rev. B **67**, 205310 (2003).

[31] T. Chakraborty and P. Pietiläinen, Phys. Rev. B **71**, 113305 (2005).

[32] M. A. Eriksson, M. Friesen, S. N. Coppersmith, R. Joynt, L. J. Klein, K. Slinker, C. Tahan, P. M. Mooney, J. O. Chu, and S. J. Koester, Quantum Inf. Process. **3**, 133 (2004); D. Loss, G. Burkard, and D. P. DiVincenzo, J. Nanopart. Res. **2**, 401 (2000); R. Hanson, L. H. Willems van Beveren, I. T. Vink, J. M. Elzerman, W. J. M. Naber, F. H. L. Koppens, L. P. Kouwenhoven, and L. M. K. Vandersypen, Phys. Rev. Lett. **94**, 196802 (2005); D. Stepanenko and N. E. Bonesteel, *ibid.* **93**, 140501 (2004).

[33] S. Bandyopadhyay, Phys. Rev. B **61**, 13813 (2000).

[34] S. Cortez, O. Krebs, S. Laurent, M. Senes, X. Marie, P. Voisin, R. Ferreira, G. Bastard, J. M. Gerard, and T. Amand, Phys. Rev. Lett. **89**, 207401 (2002).

[35] D. Grundler, Phys. Rev. Lett. **84**, 6074 (2000); C.-M. Hu, J. Nitta, T. Akazaki, H. Takayanagi, J. Osaka, P. Pfeffer, and W. Zawadzki, Physica E (Amsterdam) **6**, 767 (2000); C.-M. Hu, J. Nitta, T. Akazaki, H. Takayanagai, J. Osaka, P. Pfeffer, and W. Zawadzki, Phys. Rev. B **60**, 7736 (1999); Y. Sato, T. Kita, S. Gozu, and S. Yamada, J. Appl. Phys. **89**, 8017 (2001); J. Nitta, T. Akazaki, H. Takayanagi, and T. Enoki, Phys. Rev. Lett. **78**, 1335 (1997).

[36] Y. A. Bychkov and E. I. Rashba, J. Phys. C **17**, 6039 (1984).

[37] H. A. Bethe and E. E. Salpeter, *Quantum Mechanics of One- and Two-Electron Atoms* (Springer, Berlin, 1957).

[38] W. Zawadzki and P. Pfeffer, Semicond. Sci. Technol. **19**, R1 (2004).

[39] X. F. Wang, P. Vasilopoulos, and F. M. Peeters, Phys. Rev. B **65**, 165217 (2002).

[40] R. J. Haug, J. Weis, R. H. Blick, K. von Klitzing, K. Eberl, and K. Ploog, Nanotechnology **7**, 381 (1996); T. Schmidt, R. J. Haug, K. von Klitzing, A. Förster, and H. Lüth, Phys. Rev. Lett. **78**, 1544 (1997).

[41] R. C. Ashoori, H. L. Stormer, J. S. Weiner, L. N. Pfeiffer, K. W. Baldwin, and K. W. West, Phys. Rev. Lett. **71**, 613 (1993).

[42] V. Halonen, P. Pietiläinen, and T. Chakraborty, Europhys. Lett. **33**, 377 (1996).

[43] P. Tonello and E. Lipparini, Phys. Rev. B **70**, 081201(R) (2004).

[44] *Semiconductors, Physics of Group IV and III-V Compounds*, edited by K.-H. Hellwege and O. Madelung Landolt-Börnstein, New Series, Group III, Vol. 17, Pt. a (Springer, Berlin, 1982).

[45] G. A. Khodaparast, R. E. Doezema, S. J. Chung, K. J. Goldammer, and M. B. Santos, Phys. Rev. B **70**, 155322 (2004).

[46] B. Jouault, G. Santoro, and A. Tagliacozzo, Phys. Rev. B **61**, 10242 (2000).

[47] D. G. Austing, S. Sasaki, K. Muraki, Y. Tokura, K. Ono, S. Tarucha, M. Barranco, A. Emperador, M. Pi, and F. Garcias, in *Nano-Physics & Bio-Electronics: A New Odyssey*, Ref. 1, Chap. 2.

[48] T. Chakraborty, V. Halonen, and P. Pietiläinen, Phys. Rev. B **43**, 14289 (1991); A. Wensauer, O. Steffens, M. Suhrke, and U. Rössler, *ibid.* **62**, 2605 (2000); J. Kolehmainen, S. M. Reimann, M. Koskinen, and M. Manninen, Eur. Phys. J. B **13**, 731 (2000); A. Harju, S. Siljamäki, and R. M. Nieminen, Phys. Rev. Lett. **88**, 226804 (2002); Z. Dai, J. Sun, L. Zhang, M. Lu, Z. Li, and S. Huang, Eur. Phys. J. B **29**, 141 (2002); Appl. Phys. Lett. **80**, 2577 (2002); A. J. Markvoort, P. A. J. Hilbers, and R. Pino, J. Phys.: Condens. Matter **15**, 6977 (2003); B. Szafran, F. M. Peeters, and S. Bednarek, Phys. Rev. B **70**, 205318 (2004); T. Hatano, M. Stopa, T. Yamaguchi, T. Ota, K. Yamada, and S. Tarucha, Phys. Rev. Lett. **93**, 066806 (2004); L.-X. Zhang, P. Matagne, J. P. Leburton, R. Hanson, and L. P. Kouwenhoven, Phys. Rev. B **69**, 245301 (2004); B. Szafran and F. M. Peeters, *ibid.* **71**, 245314 (2005).

[49] J. J. Palacios and P. Hawrylak, Phys. Rev. B **51**, 1769 (1995); J. H. Oh, K. J. Chang, G. Ihm, and S. J. Lee, *ibid.* **53**, R13264 (1996); W.-Y. Ruan and H.-F. Cheung, Eur. Phys. J. B **3**, 407 (1998); H. Imamura, P. A. Maksym, and H. Aoki, Phys. Rev. B **53**, 12613 (1996); **59**, 5817 (1999); Y. Tokura, D. G. Austing, and S. Tarucha, J. Phys.: Condens. Matter **11**, 6023 (1999); B. Partoens, A. Matulis, and F. M. Peeters, Phys. Rev. B **59**, 1617 (1999); G. Burkard, G. Seelig, and D. Loss, *ibid.* **62**, 2581 (2000); B. Partoens and F. M. Peeters, Europhys. Lett. **56**, 86 (2001); W. Xie and P. Sun, J. Phys.: Condens. Matter **14**, 7245 (2002); S. Bednarek, T. Chwiej, J. Adamowski, and B. Szafran, Phys. Rev. B **67**, 205316 (2003); D. Bellucci, M. Rontani, F. Troiani, G. Goldoni, and E. Molinari, *ibid.* **69**, 201308 (2004); M. Rontani, S. Amaha, K. Muraki, F. Manghi, E. Molinari, S. Tarucha, and D. G. Austing *ibid.* **69**, 085327 (2004); G. Ortner, M. Bayer, Y. Lyanda-Geller, T. L. Reinecke, A. Kress, J. P. Reithmaier, and A. Forchel, Phys. Rev. Lett. **94**, 157401 (2005); D. Bellucci, F. Troiani, G. Goldoni, and E. Molinari, J. Lumin. **112**, 109 (2005).

[50] X.-Q. Li and Y. Arakawa, Phys. Rev. A **63**, 012302 (2000); J. M. Elzerman, R. Hanson, J. S. Greidanus, L. H. Willems van Beveren, S. De Franceschi, L. M. K. Vandersypen, S. Tarucha, and L. P. Kouwenhoven, Phys. Rev. B **67**, 161308(R) (2003); X.-Q. Li and Y. J. Yan, *ibid.* **65**, 205301 (2002); H. Qin, A. W. Holleitner, K. Eberl, and R. H. Blick, *ibid.* **64**, 241302 (2001); T. Hayashi, T. Fujisawa, H. D. Cheong, Y. H. Jeong, and Y. Hirayama, Phys. Rev. Lett. **91**, 226804 (2003); S. Vorojtsov, E. R. Mucciolo, and H. U. Baranger, Phys. Rev. B **69**, 115329 (2004); J. Gorman, E. G. Emiroglu, D. G. Hasko, and D. A. Williams, Phys. Rev. Lett. **95**, 090502 (2005).

[51] H. Sasakura, S. Adachi, S. Muto, T. Usuki, and M. Takatsu, Semicond. Sci. Technol. **19**, S409 (2004).

[52] M. Stone, H. W. Wyld, and R. L. Schult, Phys. Rev. B **45**, 14156 (1992).

[53] E. R. Davidson, Comput. Phys. **7**, 519 (1993).